Available online at www.sciencedirect.com

ScienceDirect

Solar Energy 98 (2013) 523–542

SOLAR ENERGY

www.elsevier.com/locate/solener

Improving ice productivity and performance for an activated carbon/methanol solar adsorption ice-maker

Naef A.A. Qasem, Maged A.I. El-Shaarawi *

Mechanical Engineering Department, King Fahd University of Petroleum & Minerals (KFUPM), Dhahran 31261, Saudi Arabia

Received 23 June 2013; received in revised form 27 September 2013; accepted 15 October 2013
Available online 14 November 2013

Communicated by: Associate Editor Ruzhu Wang

Abstract

The paper addresses the factors that can improve the performance of an activated carbon/methanol intermittent solar adsorption ice marker. It optimizes the ice maker under Dhahran climate with the MATLAB program to improve the performance and to increase the ice production per day per square meter of the solar collector. The optimizing results show that 14.1 kg of activated carbon NORIT RX3-Extra per m^2 of solar collector, double glazing cover, thin stainless steel absorber tubes with selective coating, suitable monthly collector tilt angle and suitable time for starting the cycle improve the performance. Moreover, the system can produce from 5 kg up to 13 kg of ice per day per m^2 of collector area with improved solar coefficients of performance (SCOP) of 0.12 and 0.24 in the hot and the cold days, respectively. The optimized solar refrigerator is of benefit to further application and producing ice in grid-off rural zones.

Keywords: Solar energy; Adsorption; Refrigeration; Modeling; Intermittent; Activated carbon/methanol

1. Introduction

Cooling systems have being become one of the important needed parts of our live. Most refrigeration systems are driven by electric energy. The electricity, that most of refrigeration systems depend on, is not covering all human living areas. For now, there are numerous places in grid off in rural zones. So people living in such areas need to store vaccine in their local clinics and to preserve their food. Accordingly, solar adsorption refrigeration technology has attracted some researchers since last decade because it is clean, cheap and simple for use in air conditioning, ice making, food preservation and vaccine storage. These devices rely on porous solid materials that can adsorb or desorb the vapor of refrigerant at certain conditions. An intermittent adsorptive solar ice-maker consists of adsorbent bed placed inside a solar collector for desorption the refrigerant from the sorbent material during solar time and adsorption the refrigerant that comes from the refrigerator at the night, in which the evaporator can be cold and some ice may be produced. The adsorption refrigeration systems depend critically on the working pairs. The common working pairs were investigated and compared by Critoph (1988), San and Lin (2008) and Wang et al. (2009). Askalany et al. (2012) also revised several refrigerants that work with carbon adsorbent. Adsorption refrigeration materials are carefully reviewed by Alghoul et al. (2007). The study showed the important properties of the adsorbent and adsorbate pairs used in the adsorption refrigeration systems and also determined the pair and materials which are suitable when solar energy is used as the main energy source. Activated carbon, zeolite, and silica gel are the essential common materials used as adsorbents whereas water, ammonia and methanol are the most important adsorbates.

* Corresponding author. Tel.: +966 505623917; fax: +966 38602949.
E-mail address: magedas@kfupm.edu.sa (M.A.I. El-Shaarawi).

0038-092X/$ - see front matter © 2013 Elsevier Ltd. All rights reserved.
http://dx.doi.org/10.1016/j.solener.2013.10.018

Nomenclature

A	area (m^2)
$A_{collector}$	collector area (m^2)
COP	coefficient of performance
C_p	specific heat at constant pressure ($J\ kg^{-1}\ K^{-1}$)
D	Dubinin–Astakhov constant (K^{-1})
$D1$	diameter of inner pass tube (m)
$D2$	internal diameter of absorber tube (m)
$D3$	external diameter of absorber tube (m)
D_o	surface diffusion coefficient ($m^2\ s^{-1}$)
E_a	activation energy of surface diffusion ($J\ mol^{-1}$)
ESCOP	effective solar coefficient of performance
h	specific enthalpy ($J\ kg^{-1}$)
h	heat transfer coefficient ($W\ m^{-2}\ K^{-1}$)
H	heat of desorption or adsorption per unit mass of methanol ($J\ kg^{-1}$)
I_T	incident solar radiation ($W\ m^{-2}$)
k	thermal conductivity ($W\ m^{-1}\ K^{-1}$)
L	latent heat ($J\ kg^{-1}$)
L_c	collector length (m)
L_t	adsorber tubes length (m)
M, m	mass (kg)
m_m	methanol uptake (kg)
n	Dubinin–Astakhov constant
N_g	number of glass cover
n_{tube}	number of absorber tubes
P	system pressure (Pa)
Q	heat amount (J)
R	gas constant ($J\ mole^{-1}\ K^{-1}$)
r	radius (m)
$R1$	radius of inner pass tube (m)
$R2$	internal radius of absorber tube (m)
$R3$	external radius of absorber tube (m)
$\mathbf{r_p}$	average radius of adsorbent particles (m)
SCOP	solar coefficient of performance
SCP	specific cooling power ($W\ kg^{-1}$)
T	temperature (°C or K)
t	time (s)/thickness (m)
U	overall heat transfer coefficient ($W\ m^{-2}\ K^{-1}$)
V_w	wind velocity ($m\ s^{-1}$)
W_c	collector width (m)
x	concentration ratio of adsorbate inside adsorbent ($kg\ kg^{-1}$)
x_o	maximum limit of mass adsorbed ($kg\ kg^{-1}$)

Greek symbols

Δ	difference/change
τ	transmittance
α	absorptivity
ε	emissivity
σ	Stefan Boltzmann constant ($W\ m^{-2}\ K^{-4}$)
β	collector tilt angle (degree)
ρ	density ($kg\ m^{-3}$)

Subscripts

1, 2, 3, 4	processes terminal locations
ac	activated carbon
a	adsorption (at end cycle)
amb	ambient
b	back
con	condenser
d	desorption (at end generation)
e	evaporator
eq	equivalent
g	generation/glass
i	insulation
ice	ice
is	collector side insulation
L	collector overall
m	methanol
max	maximum
min	minimum
pw	external wall of the adsorber tube
s	side
sa	starting adsorption
sat	saturated
sd	starting desorption
sol	solidification
t	top
w	water
wm	water tank metal

According to working pair comparisons, for low-grade temperature sources as solar energy using flat collectors, the appropriate pairs for cooling purposes are activated carbon/methanol and zeolite/water, Alghoul et al. (2007). However the zeolite/water pair is not utilized for freezing. So the suitable pair that can be used to produce ice powered by solar radiation is activated carbon/methanol. Activated carbon is a substance of crystalline form having large internal pore structures with surfaces greater than 500 $m^2\ g^{-1}$. The word activation basically means creating pores in a nonporous material such as: coal, lignite, wood, nut shells and synthetic polymers by means of chemical reactions, Askalany et al. (2012). There are many forms of activated carbon such powders, granulated, molecular sieves and carbon fibers, Srivastava and Eames (1998). The issue that appears with using activated carbon/methanol is the decomposition of methanol greater than 150 °C Eric (1998) and also greater than 120 °C if the copper tubes are used as absorbers, Alghoul et al. (2007). The decomposition of methanol is higher by use aluminum alloy material as absorbers (Eric, 1998).

Vasta et al. (2008) simulated an activated carbon/methanol adsorptive ice-maker system by use a flat plate solar

collector of 1.5 m^2 that contained 13 concentric tubes filled with 37 kg of activated carbon and about 10.5 kg of methanol for simulation according to Messina, Italy, climatic conditions (38°12′N, average useful solar radiation was about 520 W m^{-2} for June and about 250 W m^{-2} for December). For the most part of the year (from April to October), a daily ice production of 5 kg could be produced. This amount decreased to 4 kg in February and March. The coldest months in the year (January, November and December) had the amount of 2.0–3.5 kg. The net solar coefficient of performance (SCOP) had a minimum value of 0.045 in July, but the maximum one was about 0.11 in January, with an annual mean of 0.07. Zhao et al. (2008) used activated carbon/methanol to introduce a mechanical and experimental freeze proof solar adsorption cooling tube. The collector was constructed as outer tube, center tube and vacuum tube were made of hard borosilicate glass. The maximum temperature generated by the system was about 110 °C whereas the evaporator temperature reached −4 °C below zero. The device achieved 87–99 kJ of cooling capacity and a SCOP of 0.11. Hassan et al. (2011) via a theoretical simulation of a solar adsorption refrigerator assumed the effective thermal conductivity of the adsorbent bed and the system pressure as variable parameters. The results showed that the change in the effective thermal conductivity of reactor is very small (between 0.5 and 0.528 W m^{-1} K^{-1}) and the system pressure during adsorption and desorption processes was almost constant. The maximum solar coefficient of performance reached was 0.2 under Canada's climate on 30th June, 2009.

The experimental study for a solar adsorptive ice-maker by Leite et al. (2007) used methanol charcoal pair (21 kg of activated carbon and 6 kg of methanol). The collector bed was made of 9 multi tubular with an opaque black absorber surface and transparent insulation material (TIM) at top and bottom covers to minimize heat losses during desorption process under climate conditions of Brazil. Three cycles had been examined with different conditions: first condition was a clear sky, second one with partially cloudy sky, and finally under entirely cloudy sky. The study showed many features that had significant effects on the performance as degree of cloudy sky during the night. The maximum generating temperatures were 100.1, 87.3 and 92.7 °C enabled to produce 6.05, 2.10 and 0 kg of ice per square meter of the collector for the three cycles of clear sky, partially cloudy and overcast nights, respectively. Leite compared his study with TIM cover and using water for condensation with Medini et al. (1991) who used a single glazing cover and selective surface for absorber that produced 5 kg of ice per m^2 with SCOP equaled 0.15. The TIM technique reduces the top heat loss coefficient from 5 W m^{-2} K^{-1} to 1.34 W m^{-2} K^{-1}.

The analysis of the cooling and adsorption processes was investigated by Ogueke and Anyanwu (2009). The study showed that low condenser pressure increases the adsorption process while the evaporator pressure should be high to increase the adsorption process. They found also the optimum value of initial concentration of methanol was 0.21 kg kg^{-1} to obtain the best adsorbing of adsorbate (the maximum concentration was about 0.29 kg kg^{-1}). The produced ice increased from 0 kg per kg of adsorbent to about 0.4 kg.

Li and Wang (2003) studied theoretically and experimentally heat and mass transfer in an adsorbent bed for a flat plate solar adsorption ice-maker. Ten kg of methanol and 42 kg of activated carbon were used in a rectangular adsorbent bed of 1.5 m^2 solar collector. The experimental analysis was done by constructing a device in lab and simulating the solar radiation by means of quartz lamps. The investigation showed that the numerical results from the theoretical study were in agreement with the experimental results at SCOP of 0.125 and 0.132 and amounts of produced ice were 8 and 7.8 kg for 30.24 and 29 MJ of incident solar radiation, respectively.

Chekirou et al. (2007) studied theoretically the heat and mass transfer in tubular adsorbent filled with activated carbon AC-35 saturated with methanol. They showed that SCOP was 0.13, 0.172 and 0.184 and the cooling effect was 168.192, 213.661 and 229.286 kJ kg^{-1} (AC) for single glazing, double glazing and TIM system, respectively. On the other hand, the experimental work of Critoph and Tamainot-Telto (1997) showed that the double glazing cover enhanced the performance more than TIM and single glazing covers. SCOP was 0.061, 0065 and 0.071 for single cover, TIM and double cover systems, respectively.

Li et al. (2002) built a 1.5 m^2 flat plate solar adsorption ice maker using activated carbon/methanol pair. The results showed that about 4–5 kg of ice are produced by receiving about 14–16 MJ of radiation energy from quartz lamps that heated about 0.75 m^2 of solar collector while 7–10 kg of ice are produced by 28–30 MJ of radiation energy on 1.5 m^2 of the solar collector. Wang et al. (2000) used a water solar collector for heating an activated carbon/methanol adsorbent bed in a hybrid system to produce about 10 kg of ice per day per 2-m^2 of solar collector. The maximum SCOP obtained from the experimental work was about 0.144.

This study aims to increase the amount of produced ice and SCOP by investigating the main configuration parameters of the adsorption flat plate solar collector.

2. System and processes description

There is a single adsorbent bed in the intermittent solar adsorption cooling cycle. The adsorption system consists of three main parts: solar collector with adsorbent bed where activated carbon is placed, condenser and evaporator as show in Fig. 1a. The operating cycle of the system has four processes as shown in the Clapeyron diagram in Fig. 1b. The heating process (1–2) and the desorbing process (2–3) represent half the cycle while the cooling (3–4) and adsorption (4–1) processes represent the other half. During the heating period, the adsorbent bed receives heat from solar energy that raises the temperature of the pair of

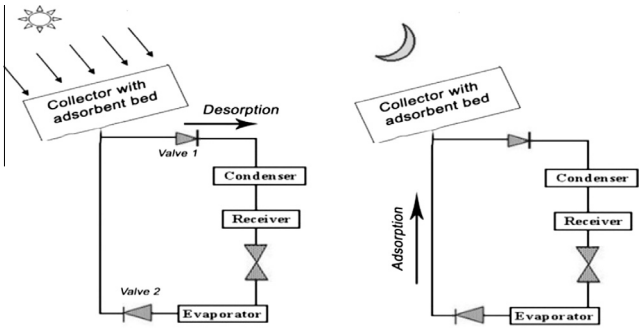

Fig. 1a. Schematic of the solar adsorption cooling system.

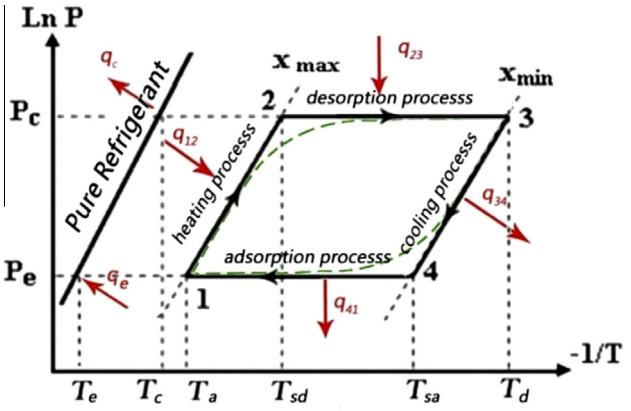

Fig. 1b. Schematic view of the adsorption process on Clapeyron diagram.

adsorbent and adsorbate as shown in Fig. 1b by line 1–2 (isosteric heating process, at constant concentration of the adsorbate = x_{max}). When the adsorbent bed pressure reaches the condenser pressure, the adsorbate vapor diffuses from the collector to the condenser and condensed there (line 2–3, desorption process at condenser pressure). So the concentration of the adsorbate in the reactor reaches the minimum value (x_{min}) at the end of this desorption process. This process is followed by cooling the generator (line 3–4, isosteric cooling process). Then, the liquid adsorbate flows from the condenser to the evaporator where it vaporizes by absorbing heat from the water to be cooled. As a result, the liquid water in evaporator becomes cold or may be converted totally or partially into ice. After that, the adsorbent adsorbs the refrigerant vapor that is coming from the evaporator (line 4–1, adsorption process at evaporator pressure). Thus, the heating and cooling processes are run at constant concentration of adsorbate while the concentration of refrigerant varies through adsorption and desorption processes.

3. System modeling

3.1. Physical description and the governing energy equations of the system

The model explains the estimation of heat and mass transfer in the three main components of the activated carbon/methanol intermittent solar adsorption cooling system. These components are the collector with adsorbent bed (reactor or generator/adsorber), the condenser and the evaporator. The activated carbon is put in an annular space between two axial tubes; the external tube is postulated to absorb the incident solar radiation, therefore it is coated by selective coating to increase the absorptivity of the surface, and the inner tube (metallic net tube) is perforated to permit methanol vapor to flow to or from the activated carbon from the evaporator or to the condenser. The system configurations are shown in Fig. 2.

3.2. Sorption concentration rate

The adsorption and desorption concentrations (x) are usually determined by Dubinin–Astakhov equation (Critoph, 1999).

$$x(T,P) = x_o \exp[-D(T\ln(P_{sat}/P))^n] \quad (1)$$

3.3. Assumptions

In the system simulation the following assumptions are utilized:

- The bed is homogenous with constant porosity and the adsorbent consists of uniform size particles.
- The vapor methanol behaves as an ideal gas.
- The desorption and adsorption occur in the vapor phase of methanol.
- The temperature of methanol and charcoal at the same point is the same.
- The variation of temperature inside the generation tubes occurs in the radial direction only.
- The convection effects within the porous bed are negligible.
- The wall of the absorber tubes is homogeneous and thin, therefore the thermophysical properties and temperature will be the same for each point.
- The specific heat of the desorbed or adsorbed methanol is considered as that of the bulk liquid methanol due to the vapor condensation on the adsorbent pores surfaces.

3.4. Adsorber (metal tube) wall temperature

The overall heat transfer coefficient of the collector (U_L) is expressed by

$$U_L = U_t + U_b + U_s \quad (2)$$

where U_t, U_b and U_s are the heat losses coefficients of the top, bottom and sides of the collector (generator/adsorber), respectively. U_s is small and can be neglected.

U_t is calculated according to Duffie and Beckman equation (Duffie and Beckman, 2006):

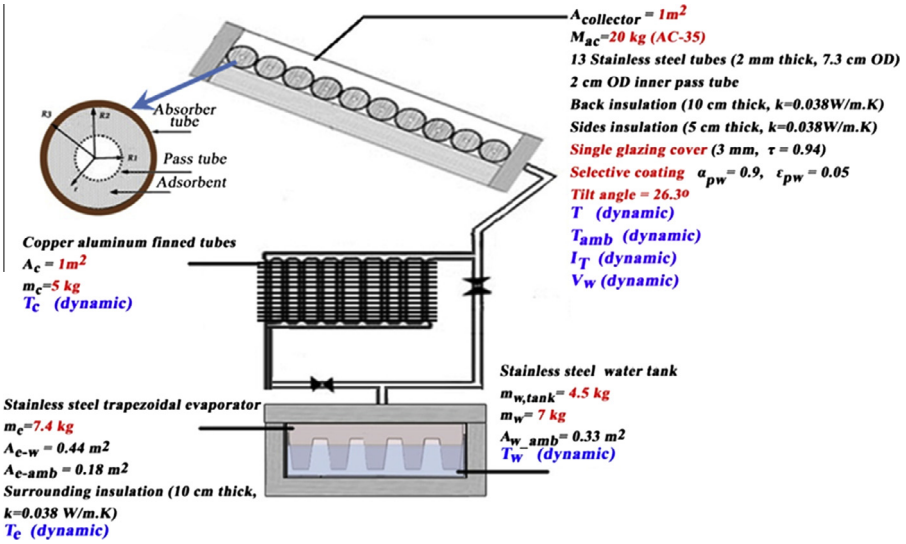

Fig. 2. Schematic details of the system.

$$U_t = \left[\frac{N_g}{\frac{c}{T_{pw}}\left(\frac{T_{pw}-T_{amb}}{Ng+f}\right)^e} + \frac{1}{h_w}\right]^{-1} + \left[\frac{\sigma(T_{pw}+T_{amb})(T_{pw}^2+T_{amb}^2)}{(\varepsilon_{pw}+0.00591N_g h_w)^{-1} + \frac{2Ng+f-1+0.133\varepsilon_{pw}}{\varepsilon_g} - N_g}\right] \quad (3)$$

where N_g is the number of glass covers, $f = (1 + 0.089\ h_w - 0.1166 h_w \varepsilon_{pw})(1 + 0.07866 N_g)$, $c = 520(1 - 0.0005\beta^2)$ for $0° < \beta < 70°$, $e = 0.430(1 - 100/T_{pw})$, β the collector tile angle (degree), ε_{pw} the emittance of the wall of the absorber tube, ε_g the emittance of the glass, T_{pw} the mean absorber tube temperature (K), T_a the ambient temperature (K), σ the Stefan–Boltzmann constant (5.6704×10^{-8}) W m^{-2} K^{-4}, h_w the wind heat transfer coefficient (W m^{-2} K^{-1}).

The back and side losses coefficients U_b and U_s depend on the insulation material and its thickness and can be evaluated by:

$$U_b = k_i/t_i \quad (4)$$

$$U_s = 2(k_i/t_{is})(L_c + W_c)t_c/((\pi/2)(D3)L_t * n_{tube}) \quad (5)$$

The outer tube wall temperature T_{pw} can be predicted by the calculation of the heat balance at the external wall of the tube ($r = R3$) as given by Eq. (6).

$$m_{pw}C_{pw}(\partial T_{pw}/\partial t) = (\tau_g \alpha_{pw})I_T(t)(D3)L_t - U_L(\pi/2) \times (D3)L_t(T_{pw} - T_{amb}) - h\pi(D2)L_t(T_{pw} - T_{r=R2}) \quad (6)$$

This equation (Eq. (6)) considers the absorbed solar radiation heat (1st term in the right side), heat losses to the ambient (2nd term in the right side) and the heat transfer to the outer layer of activated carbon/methanol (3rd term in the right side) while the lift side indicates to the heat storage in the absorber metal for small period (dt).

It might be worth mentioning here that the outer wall temperature of the tube is calculated by Eq. (6). It does not equal the ambient temperature as might seem from Eq. (2). It will be assumed equal the ambient temperature only at the initial conditions and Eq. (4) is only for calculating the heat transfer coefficient of the insulation of the collector bottom. Moreover, the areas of heat losses from the top and the bottom parts of outer wall of the tubes are the same, $((\pi/2)(D3)L_t * n_{tube})$. Different area is only associated with the collector sides and that is considered in Eq. (5). Finally, the sensible heat of water (or vapor) is not considered in the above equations as it will be considered later in the evaporator by Eq. (11) and the sensible heat of the produced ice will be considered in Eq. (13). However, with respect to the methanol inside the adsorbent bed, both sensible and adsorption/desorption heats will be considered in Eqs. (7) and (19).

3.5. Adsorbent bed

According to the previous assumptions, the adsorbent bed heat transfer is in the radial direction between the inner tube ($r = R1$) and internal surface of the external tube ($r = R2$). This heat transfer is represented by Eq. (7) taking into consideration the variation of heat storage inside the methanol due to the variation of methanol concentrations inside the activated carbon during the sorption processes. In other words, the x inside the brackets of the thermal inertia term on the left hand side of Eq. (7) is variable during the sorption processes while the values of x are constant during heating and cooling processes. The desorption/adsorption heat is also considered during the sorption processes only (2nd term in the right side).

$$\rho_{ac}[C_{p(ac)} + xC_{pm}](\partial T/\partial t) = k_{eff}[(\partial^2 T/\partial r^2) + (1/r)(\partial T/\partial r)] + \rho_{ac}\Delta H(\partial x/\partial t) \quad (7)$$

where k_{eff} is effective thermal conductivity of the bed and r represents the local radius of the adsorbent bed that varies

between the radius of the inner tube R_1 and that of the internal surface of the outer absorber tube R_2.

The kinetics of sorption $(\partial x/\partial t)$ is assumed to be governed by a linear driving force (LDF).

$$\partial x/\partial t = [(15D_o/(r_p)_2)exp(-E_a/RT)](x_{eq} - x) \quad (8)$$

where x_{eq} is the equilibrium concentration at the corresponding pressure and temperature that is calculated by Dubinin-Astakhov equation Eq. (1) and x represents the actual concentration. For activated carbon/methanol pair, the parametric reference values of Eq. (8) were estimated by Passos et al. (1989).

3.6. Condenser and evaporator

The application of the first law of thermodynamics on the condenser and the evaporator gives the following two equations, respectively:

$$M_{con}C_{p(con)}(\partial T_{con}/\partial t) = -L_{con}M_{ac}(\partial x/\partial t) - h_{con}A_{con}(T_{con} - T_{amb}) \quad (9)$$

$$[M_eC_{pe} + (M_m - xM_{ac})C_{pm}](\partial T_e/\partial t) = h_{e-w}A_{e-w}(T_w - T_e) + U_{e-amb}A_{e-amb}(T_{amb} - T_e) - L_eM_{ac}(\partial x/\partial t) \quad (10)$$

The ice should be produced if T_w reaches below zero. The following equations are used to calculate the freezing water temperature and ice mass M_{ice} as well:

when $T_w > 0$ °C, no ice produced and the energy balance equation is:

$$M_eC_{pw}(\partial T_w/\partial t) = h_{e-w}A_{e-w}(T_e - T_w) + U_{e-amb}A_{w-amb}(T_{amb} - T_w) \quad (11)$$

when $T_w = 0$ °C:

$$\mathbf{L_{sol}(\partial M_{ice}/\partial t) = h_{e-w,ice}A_{e-w}(T_e - T_w) + U_{w-amb}A_{w-amb}(T_{amb} - T_w)} \quad (12)$$

when $T_w < 0$ °C:

$$M_wC_{p(ice)}(\partial T_w/\partial t) = h_{e\text{-}ice}A_{e\text{-}w}(T_e - T_w) + U_{ice\text{-}amb}A_{w\text{-}amb}(T_{amb} - T_w) \quad (13)$$

where $h_{e\text{-}w}$ is the heat transfer coefficient between evaporator and water; it is replaced by $h_{e\text{-}w,ice}$ and $h_{e\text{-}ice}$ during and after forming ice respectively, $U_{e\text{-}amb}$ the heat transfer coefficient between the evaporator and the atmosphere, $U_{w\text{-}amb}$ the heat transfer coefficient between the water and the atmosphere and $U_{ice\text{-}amb}$ the heat transfer coefficient between the ice and the atmosphere.

3.7. Initial and boundary conditions

The variation of the climate conditions plays a basic role for the operation of any solar adsorption refrigeration system. Changes in climate conditions such as changes in the atmospheric temperature and solar insolation from hour to the next hour and from day to the next day can affect on the system performance. Such dynamic changes are taken into consideration in the present investigation and the initial conditions of the system for a new day are updated from the end of the previous day conditions.

The accompanying initial and boundary conditions can be given by:

For $t = 0$, $T = T_{pw} = T_{iw} = T_{amb}$ (at starting time of the first day), $x = x_{max}$, $P = P_e$ at the starting desorption; $T_c = T_{amb}$.

In fact at the start and during the desorption process, T_c should be a few degree higher than the ambient temperature so that the heat can be transferred from the refrigerant in the condenser to the cooling ambient.

At the starting adsorption; $M_{ice} = 0$ kg.

The boundary conditions utilized in solving Eq. (7) are as follows:

$$(\partial T/\partial r)_{r=R1} = 0 \quad (14)$$

$$-k_{eff}(\partial T/\partial r) = h(T_{pw} - T_{r=R2}) \quad (15)$$

3.8. Performance evaluation and the pertinent equations for system

The performance of the refrigeration system alone is described by the coefficient of performance of its cycle (COP) without including the solar collector performance. On the other hand, both the solar coefficient of performance (SCOP) and the effective solar coefficient of performance (ESCOP) take the solar collector field performance into consideration. The overall solar coefficient of performance (SCOP) considers the total diurnal incident solar energy as the input. The effective solar coefficient of performance (ESCOP) takes into consideration only the thermal solar energy gained by the solar collector during the heating and desorption periods.

$$\mathrm{COP} = Q_e/Q_g \quad (16)$$

$$\mathrm{SCOP} = Q_e \Big/ \int_{t=sunrise}^{t=sunset} A_cI_T(t)dt \quad (17)$$

$$\mathrm{ESCOP} = Q_e \Big/ \int_{t=sunrise}^{t=end\ of\ generation\ process} A_cI_T(t)dt \quad (18)$$

where Q_g can be estimated from sensible and desorption heat of adsorbent bed during heating and desorption processes.

$$Q_g = \int_{T_a}^{T_{sd}} \left(M_{ac}C_{p(ac)} + M_{ac}x_{max}C_{v(m)}\right)dT + \int_{T_a}^{T_d} (M_{metal}C_{metal})dT_{pw} + \int_{T_{sd}}^{T_d} \left(M_{ac}C_{p(ac)} + M_{ac}xC_{p(m)}\right)dT + \int_{T_{sd}}^{T_d} M_{ac}\Delta H dx \quad (19)$$

The evaporation heat (Q_e) is obtained by

$$Q_e = L_eM_{ac}\Delta x \quad (20)$$

where

$$\Delta x = x_{max} - x_{min} \quad (21)$$

where $I_T(t)$ is the incident solar radiation energy rate per unit collector area t is the time and A_c is the collector area. Q_e and Q_g are the cooling effect and the collector generation heat, respectively. The specific cooling power SCP (W kg^{-1}) is also used in evaluating the performance only when chilled water is produced. It is defined as the ratio between the rate of refrigeration for all cycle time per unit mass of adsorbent (activated carbon):

$$\mathrm{SCP} = Q_e / M_{ac} t_c \tag{22}$$

where M_{ac} is the mass of activated carbon (kg) and t_c is the whole cycle time.

4. Results and discussion

4.1. Validation the results

Under Dhahran climate conditions on 10–11 May 2011, the system is simulated to compare its performance results with the corresponding experimental investigation results of Medini et al. (1991) in Tunisia, as given in Table 1. Activated carbon (AC-35) has been used in the two cases. The present results are obtained for a system consisting of 0.8 m^2 single glass cover collector (with 10 stainless steel tubes, 1.93 cm adsorbent thickness and 8 cm outer adsorber diameter), air condenser (copper aluminum finned tubes: $A_c = 1$ m^2) and stainless steel trapezoidal evaporator (7.5 kg) as well as stainless steel water tank (4.2 kg). Table 1 presents the important results of the two cases to be compared such as solar coefficient of performance (SCOP), amount of methanol desorbed and condensed ($m_m(d)$), amount of produced ice (M_{ice}), maximum desorption temperature (T_d), minimum adsorption temperature (T_a), minimum evaporator temperature (T_e), maximum condenser temperature during desorption process (T_c), average atmospheric temperature during all cycle time (T_{amb}) and total incident solar radiation on the collector (I_T). The adsorbent bed parameter values such as temperature are considered the average temperature of the all radial points of the adsorbent bed from the outer surface (internal surface of outer tube) to the inner surface of the bed (the external surface of the inner tube) while the system pressure can be measured between the collector and the condenser during desorption time and between the collector and the evaporator at adsorption process. Amount of methanol desorbed could be estimated from graded vessel put below the condenser to collect condensed amount of methanol before passing to the evaporator. The values of the experimental investigation by Hassan et al. (2011) presented in Table 1 are the maximum and minimum values at terminals of processes. So, the dynamic parameters are needed for the simulation. What we did is choosing the day when the maximum and minimum values of parameters in Dhahran are close to those of Medini's investigation for the sake of comparison only. However, the simulation includes the actual hourly change in the values of the parameters. Another reason is that some minor parameters as wind speed was not mentioned in Medini's paper.

At the same incident solar radiation (I_T), collector area (A_c) and amount of activated carbon (M_{ac}) as the experimental prototype study, the first simulation (present (a), Table 1) shows T_d is higher than that of Medini prototype by about 23 °C because the 35 °C of the ambient temperature in Dhahran is much higher than the 16 °C of Tunisia at the same time of the year. Consequently, the smaller difference between the absorber and the ambient temperatures decreases heat losses from the collector. Secondly, the larger condenser temperature ($T_{c(max)} = 42.5$ °C) delays the desorption process. For the same reasons, the methanol desorbed amount ($m_m(d)$) is less (2.06 kg instead of 2.5 kg). Some of this condensed amount cannot be adsorbed during the night due to the large adsorption temperature ($T_a = 34$ °C) which impacts negatively on the system performance (as $M_{ice} = 1$ kg and SCOP = 0.1). For the same I_T, T_{amb} and T_c as the experimental values, in the present simulation results (present (b), Table 1) shows excellent agreement with the experimental performance results (as SCOP, M_{ice} and $m_m(d)$) and approximately similar parameters (as T_e, T_d and T_a) were obtained. Accordingly, the modeling code is validated.

4.2. Activated carbon type

Dubinin–Astakhov equation (Eq. (1)) shows that the sorption ability of an activated carbon depends on some physical parameters as: limited adsorption capacity (x_o), Dubinin–Astakhov constants (D and n) and other operative parameters as T and P. Among many types of activated carbon produced by some global companies, the best known eight types of activated carbon are selected in this investigation. Some of them were successfully examined with methanol as AC-35 by Medini et al. (1991), Anyanwu and Ezekwe (2003), Leite et al. (2004, 2007), and WS-480 and 207EA by Zhao et al. (2012a,b). The thermal and sorption characteristics of some others were recently examined experimentally (as x_o, D, n, density (ρ), specific heat capacity (C)) with only some limited thermodynamic analysis as: Maxsorb III by El-Sharkawy et al. (2009); Carbo Tech A35/1, G32-H, NORIT

Table 1
Comparsion between present simulation results with Medini et al. (1991) experimental results.

Study	T_d (°C)	T_a (°C)	$T_{c(max)}$ (°C)	$T_{e(min)}$ (°C)	$T_{amb(mean)}$ (°C)	I_T (MJ)	A_c (m^2)	M_{ac} (kg)	$m_m(d)$ (kg)	M_{ice} (kg)	SCOP
Medini (1991), Tunisia	90	13	30	−2	16	20	0.8	15	2.5	4.2	0.15
Present (a), Dhahran	113.5	34	42.5	−1	35	20	0.8	15	2.06	1	0.10
Present (b)	91	15	30	−1.7	16	20	0.8	15	2.6	4.5	0.153

Table 2
Characteristics of activated carbon types.

Activated carbon	x_o (kg kg^{-1})	D (K^{-1})	n	ρ (kg m^{-3})	C (kJ kg^{-1} K^{-1})
AC-35	0.33	$5.02 * 10^{-7}$	2.15	430	0.92
WS-840	0.269	$9.08 * 10^{-6}$	1.781	420	0.93
207EA	0.28	$8.45 * 10^{-7}$	2.08	460	0.92
Maxsorb III	1.24	$4.022 * 10^{-6}$	2.0	281	0.93
Carbo Tech A35/1	0.58	$1.37 * 10^{-5}$	1.76	330	0.95
G32-H	0.38	$1.94 * 10^{-8}$	2.59	370	0.95
NORIT R1-Extra	0.41	$2.19 * 10^{-7}$	2.27	420	0.95
NORIT RX3-Extra	0.425	$9.6 * 10^{-7}$	2.06	370	0.95

R1-Extra and NORIT RX3-Extra by Henninger et al. (2012). Therefore, this is the first time to model Maxsorb III, Carbo Tech A35/1, G32-H, NORIT R1-Extra and NORIT RX3-Extra with methanol under actual climate conditions. Table 2 shows the main properties of these activated carbon types. These eight types are examined in this section under Dhahran actual conditions on the worst and best days of 19th June and 19th December, respectively, to determine the best type that can be selected as the adsorbent for the adsorption ice-maker.

For the same collector configuration as shown in Fig. 2 with constant volume inside the annular space between the tubes ($V = 0.0465$ m^3), the performance for different activated carbon types is investigated as shown in Table 3. The main constructive and operative parameters of the system are as: amount of activated carbon that fills the annular space (M_{ac}), the corresponding amount of methanol for each type (M_m), maximum desorption temperature (T_d), minimum adsorption temperature (T_a), mean condenser temperature (T_c), mean condenser pressure (P_c), process or minimum evaporator pressure if solidification process is not obtained (P_e), amount of desorbed methanol during the desorption process ($m_m(d)$) and amount of adsorbed methanol during adsorption process ($m_m(a)$). On the other hand, the evaporator temperature (T_e) and amount of ice produced (M_{ice}) with the performance coefficients (COP, SCOP, ESCOP, SCP) are considered as the performance parameters of the system.

Table 3 shows the overall maximum amount of activated carbon is 21.4 kg for 207EA and the overall minimum amount of methanol (5.4 kg) for W-840 whereas Maxsorb III has the overall minimum amount of activated carbon with the overall maximum amount of methanol as 13 kg and 16.2 kg, respectively. Because of this large capacity of Maxsorb III for methanol and lower mass of adsorbent, Maxsorb III has the overall lowest maximum desorption temperatures as: 102.77 °C and 61.19 °C for the hot and the cold days, respectively, and it also has the best desorbed and adsorbed methanol amounts during both the hot and the cold days as shown in Table 3. Otherwise, the overall highest maximum desorption temperatures in the hot and the cold days are 114.16 °C and 78.8 °C, respectively, and are obtained by WS-840 that has the overall lowest methanol capacity. The other operating parameters (as T_a, T_c, P_e, P_c) have values close to each other for all the activated carbon types.

For the hot day, T_e does not go below 0 °C for WS-840, 207EA, Maxsorb III and Carbo Tech A35/1 types while the other types can produce a little amount of ice with some advantages for NORIT RX3-Extra, NORIT R1-Extra and AC-35, respectively.

The cold days show good conditions that enable all types to solidify all amount of water (7 kg). However, the evaporator temperatures show the best performance for Carbo Tech A35/1 type with $T_e = -9.6$ °C followed by NORIT RX3-Extra and NORIT R1-Extra types with $T_e = -8.44$ °C and $T_e = -8.4$ °C, respectively. Maxsorb III has the best COP, SCOP, ESCOP and SCP followed by Carbo Tech A35/1 and then NORIT RX3-Extra. However, the cooling effect that goes to water is lower for Maxsorb III. To illustrate that, as we know, the cooling effect is divided into components: the main component goes to cool the water, a second component of this heat is lost to atmosphere and other components cool the evaporator and water tank metals as well as the methanol inside the evaporator. For example, according to weather conditions, the amount of methanol inside Maxsorb III in the morning of 19th December is 10.7 kg out of 16.2 kg as shown in Fig. 3. That means there is about 5.5 kg of methanol remained inside the evaporator from previous day and then that increases to about 10.4 kg after desorption process; the increases in such amount decrease the amount of cooling heat that cools and freezes the water. Consequently, the coefficients of performance appear higher while the amount of produced ice is lower (as the hot day) or the evaporator temperature is higher if the produced ice amounts are the same (as the cold day). On the other hand, about 2.5 and 0.9 kg of methanol remained in the evaporator from previous day for Carbo Tech A35/1 and NORIT RX3-Extra, respectively.

The conclusion is that the best type that can be used for cold days is Carbo Tech A35/1 followed by NORIT RX3-Extra while NORIT RX3-Extra and NORIT R1-Extra have the best performance in hot days. Thus, the optimum performance results that can be obtained during all year days is by use of NORIT RX3-Extra.

4.3. Absorber plate and absorber coating

The suitable material for the tubes of the absorber is stainless steel due to the issues that can be caused by

Table 3
Main constructive, operative and performance parameters of the activated carbon types on 19th June and 19th December 2011.

Activated carbon	M_{ac} (kg)	M_m (kg)	Date	$T_{d(max)}$ (°C)	$T_{a(min)}$ (°C)	$T_{c(mean)}$ (°C)	$P_{c(mean)}$ (kPa)	$P_{e(mean)}$ (kPa)	$m_m(d)$ (kg)	$m_m(a)$ (kg)	$T_{e(min)}$ (°C)	M_{ice} (kg)	SCP (W kg^{-1})	COP	SCOP	ESCOP
AC-35	20	6.6	19/6	108.0	37.2	41.81	37.78	3.89	2.04	1.85	−0.3	0.04	1.11	0.28	0.077	0.096
			19/12	77.35	12.49	21.86	14.18	3.15	3.27	2.98	−7.27	7	1.93	0.41	0.150	0.177
WS-840	20	5.4	19/6	114.16	37.01	41.34	36.96	4.33	1.79	1.70	1.49	0	1.06	0.29	0.071	0.090
			19/12	81. 81	12.5	21.67	14.03	3.27	3.22	2.94	−6.32	7	1.91	0.41	0.149	0.173
207EA	21.4	6	19/6	109.38	37.12	41.67	37.50	3.95	1.95	1.79	0.03	0	1.02	0.28	0.075	0.093
			19/12	78.8	12.49	21.69	14.06	3.25	3.19	2.94	−6.32	7	1.78	0.40	0.148	0.174
Maxsorb III	13	16.2	19/6	102.77	37.48	42.49	39	4.3	2.96	2.67	1.38	0	2.37	0.37	0.107	0.130
			19/12	61.19	13.93	23.68	15.67	3.38	4.92	3.49	−7	7	3.22	0.39	0.164	0.200
Carbo Tech A35/1	15.35	8.9	19/6	110.27	37.16	41.81	37.77	4.06	2.22	2.05	0.47	0	1.63	0.33	0.086	0.106
			19/12	72.73	12.64	22.73	14.86	3.0	4.01	3.26	−9.6	7	2.68	0.41	0.160	0.190
G32-H	17.2	6.5	19/6	105.57	37.04	42	38.11	3.9	2.29	1.77	−0.22	0.01	1.24	0.26	0.074	0.092
			19/12	78.73	12.37	21.42	13.89	3.23	3.12	2.9	−5.86	7	2.2	0.41	0.148	0.175
NORIT R1-Extra	19.5	8	19/6	104.84	37.36	42.09	38.26	3.88	2.21	1.95	−0.35	0.07	1.18	0.28	0.079	0.099
			19/12	74.23	12.56	22.2	14.45	3.06	3.42	3.05	−8.4	7	2.0	0.4	0.150	0.180
NORIT RX3-Extra	17.2	7.3	19/6	107.51	37.29	41.92	37.95	3.88	2.14	1.9	−0.34	0.08	1.33	0.29	0.079	0.099
			19/12	76.52	12.49	22.09	14.36	3.04	3.4	3.04	−8.44	7	2.28	0.41	0.153	0.180

use other metals such as methanol decomposition with copper and aluminum. Furthermore, thin stainless steel tubes can handle the pressure in which the system operates under vacuum. Oppositely, the stainless steel surface has a low absorptivity to solar radiation. Therefore, the tubes should by covered or coated by high absorptivity and low emissivity material such as chrome-black selective layer type AS+(produced by Energie Solarine SA, Switzerland) with high absorptivity $\alpha_{pw} = 0.95$ and low emissivity $\varepsilon_{pw} = 0.07$. In this section, the effects of metal tubes thickness and absorptivity and emissivity of coating on the system behavior and performance are investigated, consecutively, on the typical hot day of 19th June.

Table 4 shows the parameters and performance behavior by changing the absorber thickness from 1 mm to 4 mm at the same collector configurations that were described before. It is clear that, increasing the thickness (from 1 to 4 mm) reflects negatively on all main parameters since the desorption temperature decreases from about 109 °C to about 104 °C.

Moreover, the desorbed and adsorbed amount of methanol decreases slightly from about 2.3 and 2 kg to about 2 and 1.8 kg, respectively, due to that decreases in the desorption temperatures and also the decreases in the amount of activated carbon from about 17.8 kg to about 16.3 kg as well. Correspondingly, the amount of produced ice decreases from about 0.3 kg to 0 kg with the evaporator temperature varying between −0.44 and 0.88 °C, respectively. COP, SCOP, ESCOP and SCP also decrease (due to that change in the metal thickness) from about 0.34, 0.083, 0.0107 and 1.36 (W kg^{-1}) to about 0.23, 0.074, 0.09 and 1.31 (W kg^{-1}), respectively.

Fig. 4 represents the effect of the metal thickness on M_{ice} and SCOP as given by the result shown in Table 4. Thus, the metal thickness should be as small as possible to lower the thermal inertia and hence enhance the performance of the system.

The coating properties (α_{pw} and ε_{pw}) are very important in improving the system performance. Tables 6 and 7 present the operating and performance parameters that are affected by changing the absorptivity (α_{pw}) between 0.3 and 0.95 at constant emissivity ($\varepsilon_{pw} = 0.1$), and changing emissivity (ε_{pw}) from 0.05 to 0.9 at constant absorptivity ($\alpha_{pw} = 0.9$), respectively, while taking the metal thickness as 1 mm.

The absorptivity values in Table 5 start from 0.3 because there is no desorption can be obtained below this value. The desorbed methanol amount that is associated with $\alpha_{pw} = 0.3$ is as low as about 0.19 kg. For this almost no desorption (in case $\alpha_{pw} = 0.3$), one can find the adsorbed methanol amount during the night is 0.78 kg with SCOP = 0.033 as shown in Table 5. This amount of adsorbed methanol (0.78 kg) comes from about 1.47 kg remained inside the evaporator from the previous day. The increase in the absorptivity values enable adsorbent to be heated more, hence desorbs more and adsorbs

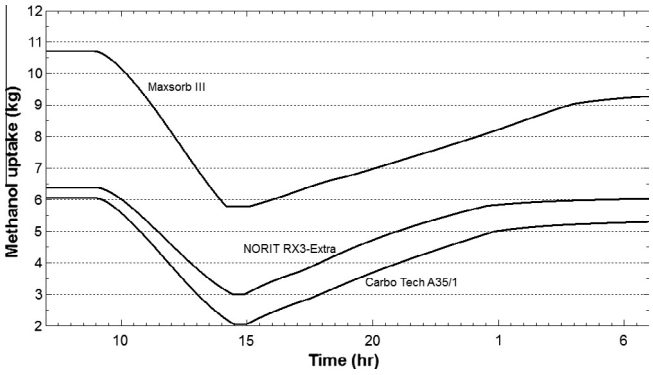

Fig. 3. Methanol uptake (mm) for three types of activated carbon for 19th December.

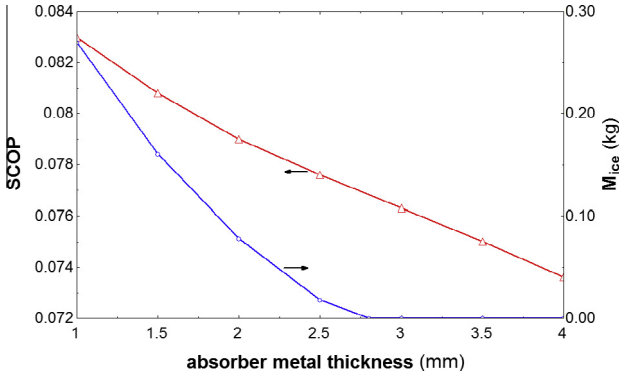

Fig. 4. Effect of metal thickness on the performance.

good quantities of methanol. Moreover, T_e, M_{ice}, SCOP, ESCOP and SCP increase with improving coating absorbance as shown in Table 5. COP alone shows negative impression with increases in the absorptivity values of metal surface, this is because of existing some of adsorption heat during the night due to the availability of methanol inside the evaporator from the previous day and the day generation heat is small with lower absorptivity values; the COP as defined before is the cooling effect divided by the generation heat.

Table 6 shows the effect of absorber emissivity on the main operating and performance parameters of the system at $\alpha_{pw} = 0.9$. Unlike effects of the metal absorptivity, the decreases in metal surface emissivity values enhance the behavior and performance of the system due to minimizing the heat losses from collector. It is obvious that, the lower surface emissivity the better is the performance. For $\varepsilon_{pw} = 0.05$, T_d is high as 108.88 °C, $m_m(d)$ is about 2.3 kg, $m_m(a)$ is 2 kg, M_{ice} is about 0.3 kg with $T_e = -0.44$ °C and SCOP is about 0.083.

Now, if the selective coating is chosen as chrome-black selective layer type AS + ($\alpha_{pw} = 0.95$ and $\varepsilon_{pw} = 0.07$) to cover stainless steel tubes with 1 mm thick, T_d increases to about 111.22 °C with about 2.44 kg and 2.13 kg of desorbed and adsorbed amounts of methanol. In addition, M_{ice}, T_e, COP, SCOP, ESCOP and SCP are improved to about 0.65 kg, −0.49 °C, 0.35, 0.089, 0.114 and 1.46 W kg^{-1}, respectively.

4.4. Adsorbent bed thickness (amount of activated carbon)

The amount of activated carbon, that fills the annular gaps between tubes, impacts strongly on the performance of the system. Large amount of activated carbon leads to slow adsorbent heating during the generation process and that affects negatively the performance. Similarly, a little amount of activated carbon increases the rates of heating and adsorption processes but with lower amounts of desorbed and adsorbed methanol.

In order to investigate the effects of the activated carbon (NORIT RX3-Extra) amounts under the worst day of the year (19th June), the diameter of the absorber tube is varied while fixing the inner pass tube diameter ($D1 = 2$ cm). The thickness of the absorber tube is taken as 1 mm coated with chrome-black selective layer ($\alpha_{pw} = 0.95$ and $\varepsilon_{pw} = 0.07$) and the other system configurations are taken as shown in Fig. 2. The internal radius of the absorber ($R2$) increases to increase the annular space ($dR = R2 - R1$) from about 1 to about 4 cm for filling 1 m^2 of collector by about 8.32–27.39 kg of NORIT RX3-Extra and about 3.54 kg to about 11.64 kg of methanol, respectively as shown in Table 7.

Table 7 shows that increasing M_{ac} leads to a decrease in T_d (from 128.07 °C to 101.37 °C) with increases in the amount of desorbed and adsorbed methanol from about 1.71 and 1.58 kg to about 2.58 and 2.36 kg, respectively. The better performed results are obtained between dR equals 1.5 and 2.0 cm. Therefore, Table 7 displays more refined values in

Table 4
Effect of absorber tube thickness on the system operating and performance parameters.

t_{metal} (mm)	M_{ac} (kg)	M_m (kg)	T_d (°C)	T_a (°C)	$T_{c(mean)}$ (°C)	$P_{c(mean)}$ (kPa)	$P_{e(mean)}$ (kPa)	$m_m(d)$ (kg)	m_m (a)(kg)	$T_{e(min)}$ (°C)	M_{ice} (kg)	COP	SCOP	ESCOP	SCP (W kg^{-1})
1	17.75	7.54	108.88	37.52	41.94	38.0	3.88	2.30	2.0	−0.44	**0.27**	0.34	**0.083**	0.107	1.36
1.5	17.50	7.44	108.20	37.42	41.94	38.0	3.88	2.23	1.95	−0.40	**0.16**	0.32	**0.081**	0.103	1.34
2	17.26	7.37	107.51	37.28	41.93	37.98	3.88	2.17	1.90	−0.35	**0.08**	0.29	**0.079**	0.099	1.33
2.5	17.02	7.24	106.08	37.15	41.91	37.94	3.90	2.11	1.87	−0.26	**0.02**	0.28	**0.078**	0.096	1.32
3	16.8	7.14	106.02	37.23	41.88	37.90	3.97	2.06	1.84	−0.11	**0**	0.26	**0.076**	0.094	1.32
3.5	16.6	7.04	105.22	37.28	41.85	37.78	4.06	2.01	1.81	0.47	**0**	0.25	**0.075**	0.091	1.32
4	16.3	6.95	104.33	37.32	41.82	37.79	4.16	1.98	1.77	0.88	**0**	0.23	**0.074**	0.089	1.31

Table 5
The effect of absorber absorptivity on system operating and performance parameters at $\varepsilon_{pw} = 0.1$.

α_{pw}	T_d (°C)	T_a (°C)	$T_{c(mean)}$ (°C)	$P_{c(mean)}$ (kPa)	$P_{e(min)}$ (kPa)	$m_m(d)$ (°C)	$m_m(a)$ (°C)	$T_{e(min)}$ (°C)	M_{ice} (kg)	COP	SCOP	ESCOP	SCP (W kg^{-1})
0.3	69.97	36.64	39.87	34.51	11.27	0.19	0.87	17.80	**0**	0.45	**0.033**	0.044	0.54
0.4	75.78	36.71	40.23	35.10	9.33	0.54	0.96	14.40	**0**	0.41	**0.041**	0.054	0.66
0.5	81.69	36.58	40.61	35.72	7.72	0.89	1.16	11.10	**0**	0.38	**0.048**	0.064	0.79
0.6	87.75	36.83	40.96	36.31	6.41	1.23	1.35	7.92	**0**	0.36	**0.056**	0.074	0.92
0.7	93.95	36.88	41.21	36.87	5.34	1.56	1.55	4.91	**0**	0.35	**0.064**	0.084	1.05
0.8	100.35	36.93	41.58	37.37	4.49	1.88	1.74	2.07	**0**	0.34	**0.072**	0.094	1.18
0.9	106.97	37.10	41.89	37.82	3.88	2.18	1.92	−0.35	**0.07**	0.34	**0.080**	0.102	1.30
0.95	110.03	37.64	41.99	38.08	3.88	2.37	2.06	−0.47	**0.44**	0.34	**0.086**	0.110	1.40

Table 6
The effect of absorber emissivity on system operating and performance parameters at $\alpha_{pw} = 0.9$.

ε_{pw}	T_d (°C)	T_a (°C)	$T_{c(mean)}$ (°C)	$P_{c(mean)}$ (°C)	$P_{e(min)}$ (°C)	$m_m(d)$ (kg)	$m_m(a)$ (kg)	$T_{e(min)}$ (°C)	M_{ice} (kg)	COP	SCOP	ESCOP	SCP (W kg^{-1})
0.05	108.88	37.52	41.94	38.0	3.88	2.30	2.0	−0.44	**0.27**	0.34	**0.083**	0.107	1.36
0.1	106.97	37.10	41.89	37.82	3.88	2.18	1.92	−0.35	**0.07**	0.34	**0.080**	0.102	1.30
0.2	103.66	37.0	41.70	37.59	4.12	2.04	1.83	0.70	**0**	0.34	**0.076**	0.099	1.24
0.3	100.94	36.83	41.59	37.40	4.40	1.92	1.76	1.78	**0**	0.34	**0.073**	0.096	1.19
0.4	98.53	36.77	41.48	37.20	4.69	1.82	1.67	2.77	**0**	0.34	**0.070**	0.091	1.15
0.5	96.26	36.72	41.37	37.0	4.97	1.71	1.63	3.73	**0**	0.35	**0.067**	0.089	1.11
0.6	94.01	36.67	41.25	36.80	5.28	1.61	1.56	4.72	**0**	0.35	**0.065**	0.086	1.06
0.7	91.71	36.62	41.12	36.59	5.63	1.49	1.49	5.76	**0**	0.35	**0.062**	0.083	1.02
0.8	89.27	36.56	40.98	36.35	6.03	1.36	1.42	6.89	**0**	0.36	**0.059**	0.079	0.97
0.9	86.65	36.51	40.83	36.08	6.50	1.22	1.34	8.15	**0**	0.36	**0.056**	0.075	0.91

Table 7
The effect of the adsorbent bed thickness on system operating and performance parameters.

dR (cm)	M_{ac} (kg)	M_m (kg)	T_d (°C)	T_a (°C)	$T_{c(mean)}$ (°C)	$P_{c(mean)}$ (kPa)	$P_{e(mean)}$ (kPa)	$m_m(d)$ (kg)	$m_m(a)$ (kg)	$T_{e(min)}$ (°C)	M_{ice} (kg)	COP	SCOP	ESCOP	SCP (W kg^{-1})
1.0	8.32	3.54	128.07	36.95	40.95	36.30	3.91	1.71	1.58	0.31	**0.04**	0.39	**0.073**	0.098	2.55
1.5	11.76	5.0	120.55	37.26	41.52	37.28	3.87	2.10	1.90	0.54	**0.76**	0.39	**0.086**	0.112	2.13
1.6	12.42	5.28	119.32	37.15	41.60	37.40	3.87	2.15	1.95	0.55	**0.83**	0.39	**0.087**	0.114	2.05
1.7	13.08	5.71	118.13	37.25	41.68	37.60	3.87	2.20	2.0	0.54	**0.86**	0.39	**0.089**	0.115	1.97
1.8	13.73	5.84	117.02	37.33	41.75	37.67	3.87	2.25	2.02	0.52	**0.88**	0.38	**0.089**	0.116	1.89
1.9	14.38	6.11	115.99	37.42	41.80	37.77	3.87	2.29	2.05	0.50	**0.89**	0.38	**0.090**	0.116	1.82
2.0	15.03	6.39	115.02	37.50	41.85	37.86	3.87	2.32	2.07	0.47	**0.88**	0.37	**0.090**	0.116	1.75
2.5	18.19	7.73	110.78	37.80	42.05	38.21	3.87	2.44	2.14	0.50	**0.63**	0.35	**0.089**	0.114	1.42
3.0	21.30	9.05	107.31	37.79	42.17	38.40	3.87	2.51	2.19	0.45	**0.27**	0.32	**0.086**	0.109	1.17
3.5	24.36	10.35	104.29	37.74	42.23	38.51	3.90	2.55	2.26	0.27	**0.01**	0.30	**0.083**	0.106	1.0
4.0	27.39	11.64	101.37	38.73	42.27	38.57	4.18	2.58	2.36	0.94	**0**	0.28	**0.082**	0.103	0.87

this range of dR with 1 mm increment to show the optimum results. The results of Table 7 are presented in Fig. 5, which shows that the optimal performance results are obtained by taking $M_{ac} = 14.09$ kg. Thus, for about 14.1 kg of NORIT-RX3-Extra and about 6 kg of methanol, about 0.9 kg of ice (optimum) can be produced at evaporator temperature $T_e = -0.51$ °C and the corresponding COP, SCOP, ESCOP and SCP are 0.38, 0.09 (optimum), 0.116 (optimum) and 1.85 (W kg^{-1}), respectively.

4.5. Glazing cover number and types

While the main purpose of the glazing cover is to reduce heat losses from the solar collectors, the glazing cover actually does not permit all sun radiation to reach absorber. It has a specific value of transmittance that should be as high as possible. Single glazing cover (of 3 mm thick), double glazing cover (each sheet is 3 mm thick) and transparent insulation material (TIM) are investigated in this section. The collector configuration is as obtained before (about 14.1 kg of NORIT RX3-Extra, 1 mm thick of stainless steel absorber with selective coating ($\alpha_{pw} = 0.95$ and $\varepsilon_{pw} = 0.07$)).

The sheets type of single and double glazing covers is water white glass (low iron glass, $(\tau_g)_{max} = 0.94$) while TIM is an 8 cm thick polycarbonate honeycomb with 3 cm as the equivalent radius of the cells and 3 mm thick for the top and the bottom bases.

Fig. 6 shows the glass transmissivity and the absorber absorptivity products ($\tau_g\alpha_{pw}$) of the three glazing cover systems on the typical hot day of 19th June. It is obvious that

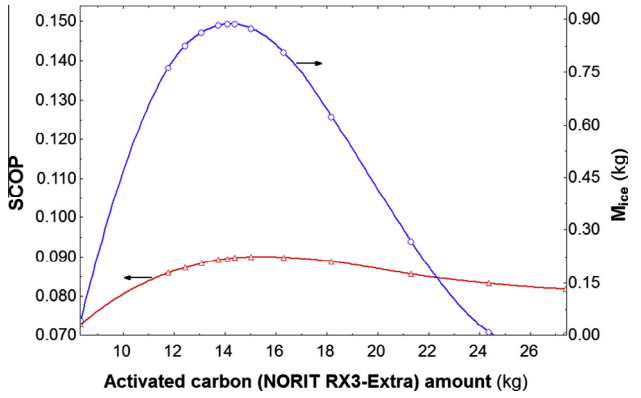

Fig. 5. The effect of the activated carbon NORIT RX3-Exta amount (M_{ac}) on the performance.

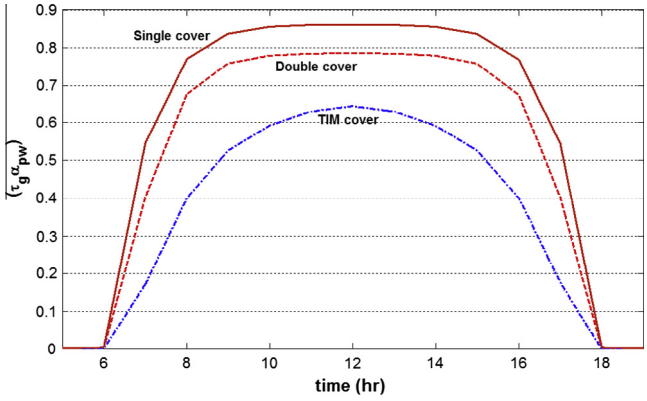

Fig. 6. Transmissivity absorptivity product ($\tau_g \alpha_{pw}$) of the three glazing cover systems.

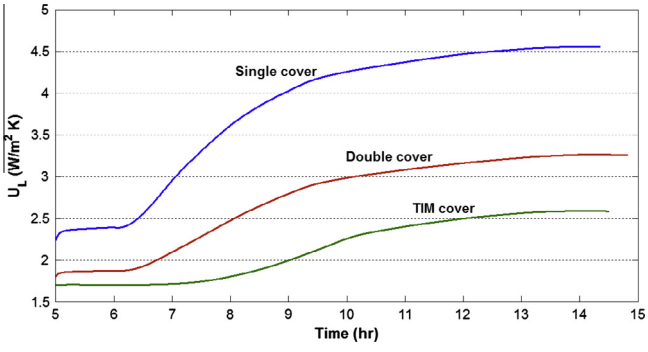

Fig. 7. Overall collector heat loss coefficient (U_L) during heat generation time of the three glazing cover systems.

the single cover system has the higher value ($(\tau_g \alpha_{pw})_{max} = 0.86$) and the second high value is for double glazing system ($(\tau_g \alpha_{pw})_{max} = 0.786$) while the TIM has the lowest value ($(\tau_g \alpha_{pw})_{max} = 0.646$). Correspondingly, TIM system absorbs a less radiation whereas the single cover system can absorb the best amount of solar radiation. However, the advantage of TIM is ability to minimize the heat losses. TIM has the lowest values of collector heat loss coefficient ($U_L = 1.7$–$2.6\ \mathrm{W\ m^{-2}\ K^{-1}}$) compared to the single cover ($U_L = 2.8$–$4.6\ \mathrm{W\ m^{-2}\ K^{-1}}$) and the double cover

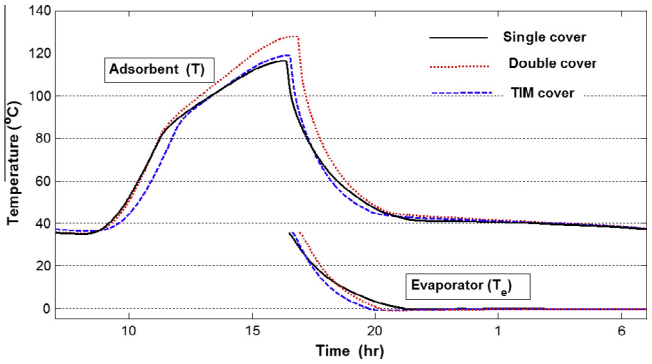

Fig. 8. Adsorbent (T) and evaporator (T_e) temperatures of the three glazing cover systems.

Table 8
Effect of glazing cover systems on operating and performance parameters.

Parameters	Single cover	Double cover	TIM cover
T_d (°C)	116.41	127.91	118.84
T_a (°C)	37.6	37.65	37.11
$T_{c(mean)}$ (°C)	41.78	42.12	42.07
$T_{e(min)}$ (°C)	−0.51	−1.16	−0.98
$P_{c(mean)}$ (kPa)	37.7	38.33	38.2
$P_{e(mean)}$ (kPa)	3.87	3.79	3.82
$m_m(d)$ (kg)	2.27	2.76	2.15
$m_m(a)$ (kg)	2.04	2.52	2.13
M_{ice} (kg)	**0.88**	**2.41**	**2.01**
COP	0.38	0.40	0.41
SCOP	**0.089**	**0.112**	**0.094**
ESCOP	0.116	0.136	0.120
SCP (W kg^{-1})	1.85	2.31	1.93

($U_L = 1.8$–$3.75\ \mathrm{W\ m^{-2}\ K^{-1}}$) glazing systems during heating and desorption processes (generation time), as shown in Fig. 7.

For these reasonable values of ($\tau_g \alpha_{pw}$) and U_L, the maximum temperature of adsorbent (127. 91 °C) can be obtained by double glazing cover system while TIM and single glazing cover systems have closed T_d values such as 118.84 and 116.41 °C, respectively, as shown in Fig. 8 and Table 8. For these generation temperatures, the desorbed methanol is higher by double glazing system ($m_m(d) = 2.76$ kg) whereas $m_m(d)$ for single cover and TIM systems are 2.27 and 2.15 kg, respectively, as shown in Fig 9 and Table 8. Furthermore, adsorbed methanol amount $m_m(a)$ values indicate some advantages for the double gazing system (2.52 kg) followed by TIM (2.13 kg) and then the single cover system (2.04 kg), respectively. The corresponding amounts of the produced ice are about 2.41, 2.01 and 0.88 kg for the double glazing system, TIM and single glazing system, respectively, as shown in Fig. 9 and Table 8.

Table 8 shows the main operating and performance parameters, the main parameters values confirm that the double glazing system is the best type followed by TIM and then single glazing system with SCOP equals 0.112, 0.094 and 0.089, respectively.

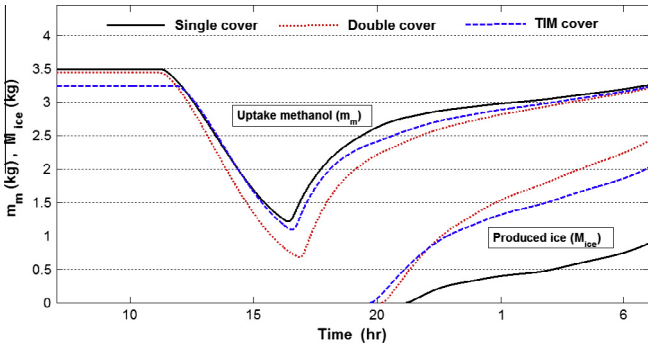

Fig. 9. Methanol uptake (mm) and amount of produced ice (M_{ice}) for the three glazing cover systems.

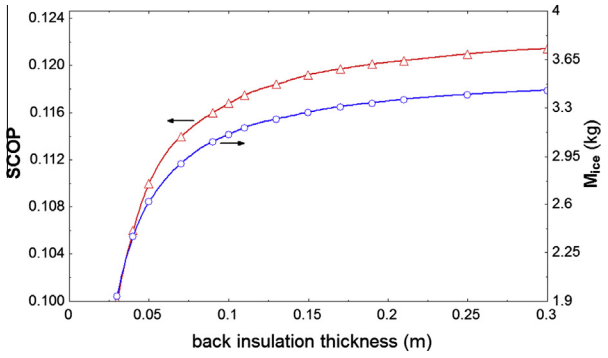

Fig. 10. Effect of back insulation thickness (t_i) on M_{ice} and SCOP.

4.6. Back insulation thickness

As the glazing cover is used to reduce heat losses from the top side of the collector, the insulation material on the sides and the rear of the collector is used for the same purpose. Fiberglass insulation is used in all previous sections to insulate the system having 10 cm thick on the rear of collector, 5 cm thick on all the collector sides and 10 cm thick for surrounding the evaporator. Fiberglass material has a low thermal conductivity (about 0.038 W m^{-1} K^{-1}) and has a capability to handle temperature more than 500 °C. Other insulation materials such as expanded polystyrene and rigid polyurethane foam have lower thermal conductivity (about 0.034 and 0.025 W m^{-1} K^{-1}), but the maximum operating temperature is as low as 75 °C and 120 °C, respectively. Polyisocyanurate insulation material (Polyiso) has lower thermal conductivity (about 0.025 W m^{-1} K^{-1}) and can serve up to 150 °C of temperature, which is suitable for activated carbon methanol systems that should avoid any temperature that exceeds 150 °C due to decomposition of methanol. If rigid polyisocyanurate foam boards are used to insulate the sides and rear of collector with fiberglass material remain only in the evaporator box walls, M_{ice}, T_e, SCOP and T_d are improved from 2.41 kg, −1.15 °C, 0.112 and 127.91 °C to about 2.78 kg, −1.30 °C, 0.117 and 131.50 °C, respectively, whereas use of polyisocyanurate in the evaporator box walls as well as in the collector enhances M_{ice} up to 3.11 kg at $T_e = -1.35$. Therefore, the effect of the collector back insulation (Polyiso) thickness on the operating and performance parameters is investigated in this section while the glazing system used is the double cover.

Table 9 represents the effect of the collector back insulation thickness (t_i) on the operating and performance parameters. Increasing t_i from 0.03 m to 0.21 m increases T_d from about 121.32 °C to about 134.34 °C and the corresponding $m_m(d)$ from 2.51 kg to 2.95 kg. Also, $m_m(a)$ increases from about 2.26 to about 2.71 at the closed values of adsorption temperatures (from 37.58 °C to 37.85 °C). According to these improvements in T_d and m_m, M_{ice} increases from 1.94 kg to 3.36 kg with a corresponding T_e varying from −0.84 to −1.45 °C. COP, SCOP, ESCOP and SCP also increase from about 0.39, 0.1, 0.124 and 2.06 (W kg^{-1}) to about 0.41, 0.12, 0.144 and 2.49 (W kg^{-1}), respectively.

Fig. 10 shows the trend of the most two important operative parameters (M_{ice}, SCOP) with t_i varies from 3 cm to 30 cm. It is clear that both M_{ice} and SCOP increase sharply for increasing the collector back insulation thickness from 3 to 10 cm and then they rise slowly. The insulation thicknesses 5 and 10 cm are always used in the literature to avoid exaggerated thickness of the collector. For that, the back collector insulation thickness is taken as 10 cm to minimize significantly the amount of the heat losses during the generation (heating and desorption) time.

Table 9
The effect of collector back insulation thickness on system operating and performance parameters.

t_i (m)	T_d (°C)	T_a (°C)	$T_{c(mean)}$ (°C)	$P_{c(mean)}$ (°C)	$P_{e(min)}$ (°C)	$m_m(d)$ (kg)	$m_m(a)$ (kg)	$T_{e(min)}$ (°C)	**M_{ice} (kg)**	COP	**SCOP**	ESCOP	SCP (W kg^{-1})
0.03	121.32	37.58	42.0	38.11	3.83	2.51	2.26	−0.84	**1.94**	0.39	**0.100**	0.124	2.06
0.05	126.73	37.71	42.10	38.30	3.80	2.72	2.48	−1.14	**2.62**	0.40	**0.110**	0.134	2.26
0.07	129.36	37.76	42.14	38.36	3.79	2.80	2.57	−1.26	**2.90**	0.41	**0.114**	0.138	2.35
0.09	130.93	37.79	42.16	38.40	3.78	2.85	2.61	−1.32	**3.06**	0.41	**0.116**	0.140	2.40
0.10	131.50	37.8	42.16	38.41	3.78	2.87	2.63	−1.35	**3.11**	0.41	**0.117**	0.140	2.41
0.11	131.97	37.81	42.17	38.42	3.77	2.88	2.64	−1.36	**3.16**	0.41	**0.118**	0.141	2.43
0.13	132.72	37.82	42.18	38.44	3.77	2.90	2.67	−1.39	**3.22**	0.41	**0.118**	0.142	2.45
0.15	133.28	37.83	42.18	38.46	3.77	2.92	2.68	−1.41	**3.27**	0.41	**0.119**	0.143	2.46
0.17	133.72	37.83	42.19	38.46	3.77	2.93	2.69	−1.43	**3.31**	0.41	**0.120**	0.143	2.47
0.19	134.06	37.84	42.19	38.46	3.77	2.94	2.70	−1.44	**3.34**	0.41	**0.120**	0.143	2.48
0.21	134.34	37.85	42.19	38.47	3.77	2.95	2.71	−1.45	**3.36**	0.41	**0.120**	0.144	2.49

Table 10
Average monthly collector tilt angle for Dhahran.

Month	1	2	3	4	5	6	7	8	9	10	11	12
Tilt angle	47.4	39.5	28.9	17.1	7.7	3.4	5.3	13.0	24.3	36.1	45.4	49.4

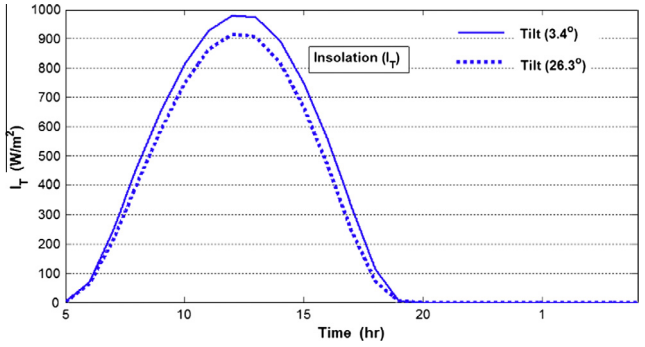

Fig. 11. Effect of collector tilt angle on incident solar radiation on collector on 19th June.

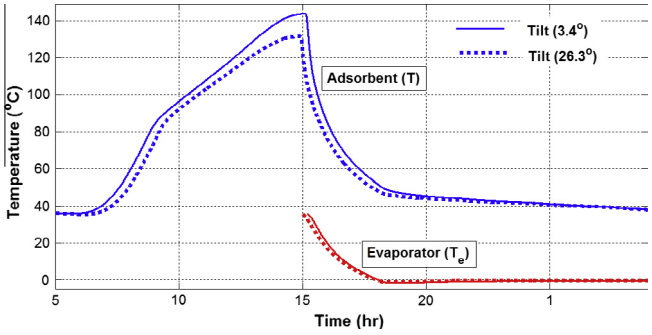

Fig. 12. Effect of collector tilt angle on adsorbent (T) and evaporator (T_e) temperatures on 19th June.

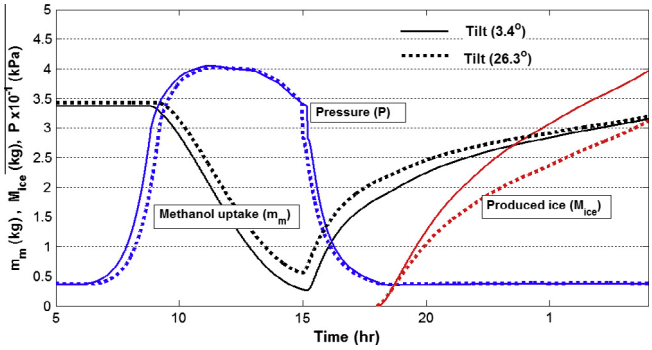

Fig. 13. Effect of collector tilt angle on methanol uptake (T_d), pressure (P) and amount of produced ice (M_{ice}) on 19th June.

4.7. Other improvements

In the previous sections, the solar collector tilt angle (β) is assumed constant at the same value of Dhahran latitude (about 26.3°). This tilt angle is suitable to absorb maximum insolation all year days if the collector is fixed without moving during all days because of the heavy weight of the collector (about 55 kg without frame). However, it is more suitable to tilt the collector at least one time every month according to the tilt angle values that are proposed in Table 10 to minimize the solar incident angle below 6° at noon (incident solar radiation will be almost perpendicular on the collector) for all months days.

The typical hot day on 19th June is selected to compare the effect of the tilt angle of the collector (at 26.3° and 3.4°) on the received solar radiation and the corresponding variation in I_T, T_d, T_e, P, M_{ice} and m_m as shown in Figs. 11–13.

Fig. 11 shows that for collector tilt equals of 26.3° and 3.4°, respectively, the maximum incident solar radiation rises from about 915.3 W m^{-2} to about 979.1 W m^{-2} and the total received radiation during a day from about 25.13 MJ m^{-2} to about 27.98 MJ m^{-2}. For this increment in the solar radiation that is caused by the suitable average monthly tilt angle (of 3.4° for June), the desorption temperature increases to about 143.94 °C instead of 131.5 °C (in the case of Tilt = 26.3°). T_e also decreases from −1.45 °C to −1.67 °C, as shown in Fig. 12and 1st and 2nd columns of Table 11.

Fig. 13 shows the effect of collector tilt angle on m_m, P and M_{ice}. Due to increasing the adsorbent temperature as shown in Fig. 12, the amounts of desorbed and adsorbed methanol increase from about 2.87 kg and 2.63 kg to about 3.1 and 2.9 kg as shown in Fig. 13 and Table 11. Therefore, the corresponding amount of produced ice increases from about 3.11 kg to about 3.96 kg at mean evaporator pressure equals 3.78 and 3.74 kPa for the collector tilts of 26.3° and 3.4°, respectively. COP, SCOP, ESCOP almost remain at the same values due to the increase in both the received heat and cooling effect while SCP increases by about 10% as shown in 1st and 2nd columns of Table 11.

The sunset in Dhahran during the hot months such as April, May, June, July and August is between 5 and 6 AM

Table 11
Effect of collector tilt angle and time offset on operating and performance parameters.

Parameters	Tilt = 26.3°	Tilt = 3.4°	Tilt = 3.4° with time offset
T_d (°C)	131.5	143.94	143.4
T_a (°C)	37.8	38.01	37.3
$T_{c(mean)}$ (°C)	42.16	42.02	42.05
$T_{e(min)}$ (°C)	−1.35	−1.67	−1.68
$P_{c(mean)}$ (kPa)	38.41	38.17	38.2
$P_{e(mean)}$ (kPa)	3.78	3.74	3.74
$m_m(d)$ (kg)	2.87	3.1	3.17
$m_m(a)$ (kg)	2.63	2.89	2.97
M_{ice} (kg)	**3.11**	**3.96**	**4.25**
COP	0.41	0.41	0.42
SCOP	**0.117**	**0.116**	**0.119**
ESCOP	0.140	0.139	0.143
SCP (W kg^{-1})	2.41	2.66	2.74

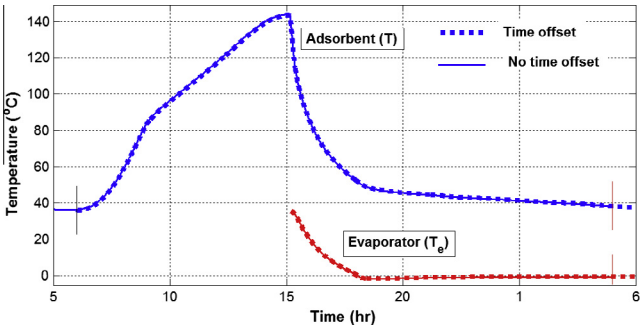

Fig. 14. Effect of time offset on adsorbent (T) and evaporator (T_e) temperatures at Tilt = 3.4° on 19th June.

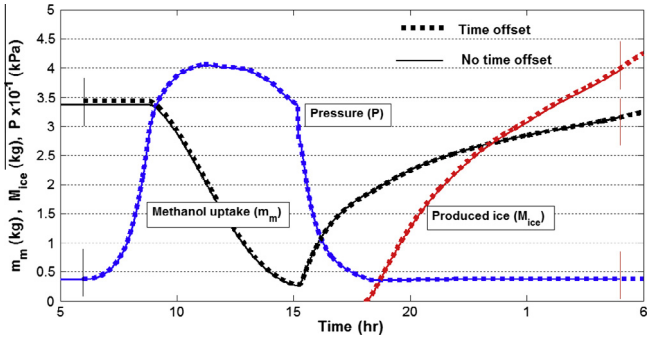

Fig. 15. Effect of time offset on methanol uptake (mm), pressure (P) and produced ice (M_{ice}) at Tilt = 3.4° on 19th June.

(solar time) and there is no actual heating during this period as shown in Fig. 14 on the typical hot day (19th June). Thus, it is suitable to start the cycle at 6 AM (solar time) on the hot days and leaving the time between sunrise and 6 AM as extra time for adsorption process to the pervious cycle to improve the amount of produced ice and other performance parameters as shown in Fig. 15 and 3rd column in Table 11. In winter days the heating starts at the sunrise time (usually after 6 AM) due to the increase in solar zenith angle, so there is no need to shifting starting time.

Figs. 14 and 15 and Table 11 show that these are no significant changes in the operative parameters due to this time offset. However the amount of ice produced increases from 3.96 to 4.24 kg and SCOP is 0.119 instead of 0.116 (in case of no time offset).

The next section concerns with these improvements (collector tilt angle and starting time offset) and all the previous improvements to show the enhanced behavior and the performance of the system.

4.8. Actual system behavior after the previous improving on the main collector parameters under Dhahran climate conditions

After all the previous suggested improvements, the system is simulated during ten consecutive days for both summer and winter to show its actual behavior and performance. The proposed collector (1 m^2) consists of 17 stainless steel tubes (1 mm thick, about 59.3 mm outer diameter and 1 m long) with 2 cm outer diameter of inner perforated pass steel tubes to handle the optimum mass of about 14.1 kg of NORIR RX3-Extra; the corresponding methanol is about 6 kg. The tubes are covered by chrome-black selective layer ($\alpha_{pw} = 0.95$ and $\varepsilon_{pw} = 0.07$); the double glazing system is selected. Rigid polyisocyanurate foam insulation is used on the sides (5 cm thick) and back (10 cm thick) of the collector as well as on the box that surrounds the evaporator (10 cm thick). The other system components data are shown in Fig. 16. The solar collector tilt angles are taken corresponding to those values shown in Table 10; the offset starting operating time is taken into consideration.

The system behavior and performance are estimated under Dhahran hot climate conditions during 10 consecutive days (from 14th to 23th of June 2011), as shown in Figs. 17–19 and Table. 12.

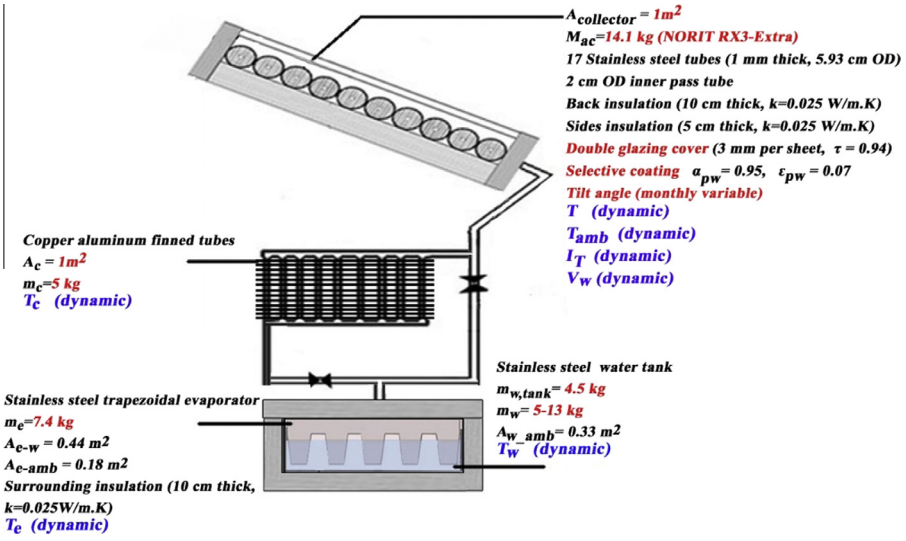

Fig. 16. System configuration details after the improvements.

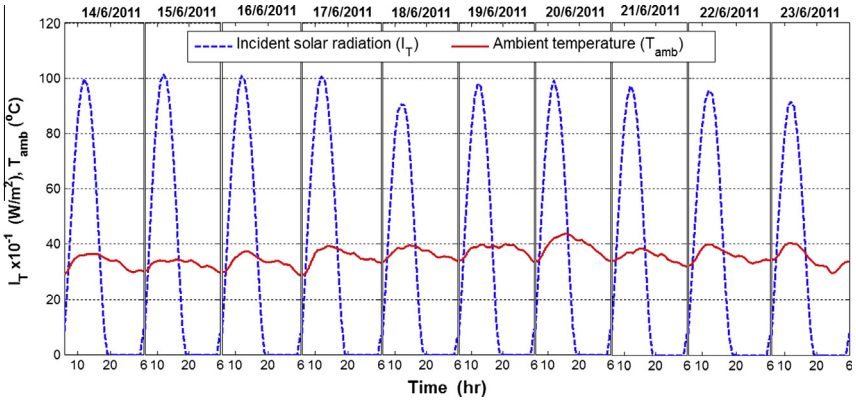

Fig. 17. Solar radiation on collector (I_T) and ambient temperature (T_{amb}) recorded in June 2011.

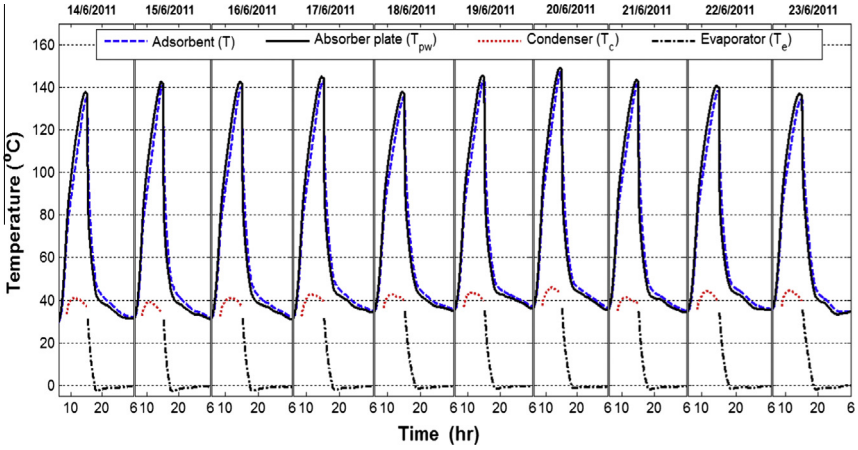

Fig. 18. Collector absorber (T_{pw}), adsorbent bed (T), condenser (T_c) and evaporator (T_e) temperatures calculated for June 2011.

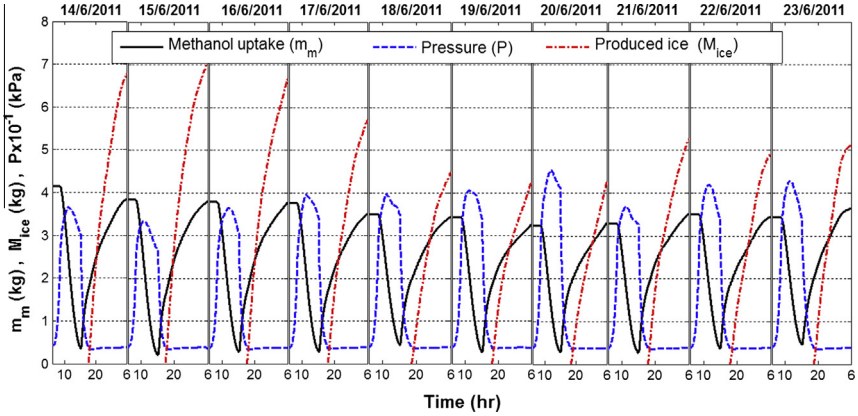

Fig. 19. Methanol uptake (mm), adsorbent bed pressure (P) and amount of produced ice (M_{ice}) calculated for June 2011.

Fig. 17 shows the incident solar radiation on suitable collector tilt (Tilt = 3.4°) from 14th to 23rd of June. Comparing the I_T values shown in Fig. 17 to those when the collector tilt angle = 26.3° during the same period affirms some increases in I_T values from about 904.4 W m^{-2} as minimum on 18th June to about 1016 W m^{-2} on 15th June as maximum instead of about 850 W m^{-2} as a minimum to 950 W m^{-2} as a maximum for the same two days. The corresponding solar radiations received during these two days times are 26.39 and 29.3 MJ m^{-2} instead of 26.28 and 23.88 MJ m^{-2}, thus improved about 10.5% and 11.5% for the two days (18th and 15th June), respectively.

The overall adsorbent temperatures are shown in Fig. 18; the maximum desorption temperature (T_d) is 135°C on 14th June as a minimum and T_d = 147.7 °C on 20th June as the maximum. Recalling that T_d should be

Table 12
System performance for June 2011.

Date	14/6	15/6	16/6	17/6	18/6	19/6	20/6	21/6	22/6	23/6
COP	0.44	0.47	0.46	0.42	0.44	0.42	0.44	0.47	0.44	0.48
SCOP	**0.140**	**0.139**	**0.137**	**0.125**	**0.127**	**0.119**	**0.120**	**0.131**	**0.130**	**0.137**
ESCOP	0.165	0.165	0.164	0.150	0.152	0.143	0.143	0.157	0.154	0.164
SCP (W kg^{-1})	3.25	3.33	2.24	2.98	2.76	2.74	2.77	2.99	2.85	2.93
***M*$_{ice}$ (kg)**	**6.77**	**7**	**6.67**	**5.69**	**4.47**	**4.25**	**4.25**	**5.26**	**4.91**	**5.1**
$m_m(d)$ (kg)	3.8	3.63	3.51	3.48	3.05	3.16	2.96	3.03	3.14	2.99
$m_m(a)$ (kg)	3.48	3.58	3.49	3.21	2.99	2.97	3.01	3.03	3.10	2.99
P_e (kPa)	3.65	3.64	3.66	3.67	3.72	3.74	3.73	3.70	3.72	3.70
P_c (kPa)	33.72	30.5	33.60	36.20	37.01	38.20	41.95	39.38	38.32	39.36

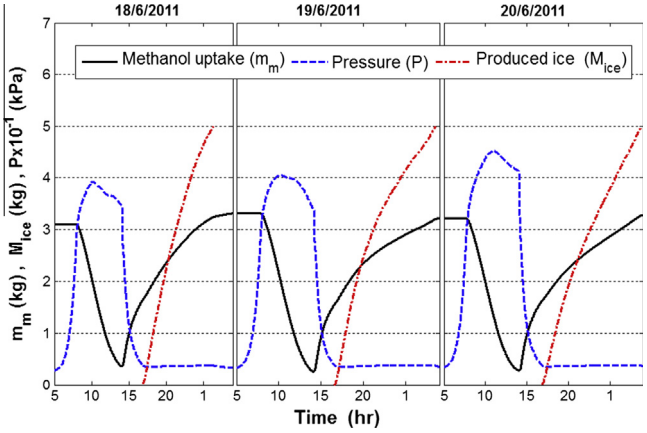

Fig. 20. Methanol uptake (mm), adsorbent bed pressure (P) and amount of produced ice (M_{ice}) calculated for 18th, 19th and 20th June 2011 (for $m_w = 5$ kg).

below 150 °C, for this reason, the previous improvements take that into consideration as shown in Fig. 18; the highest value of T_d is 147.7 °C on 20th June and the others days have lower than this value. Notice that T_c values are not changed much while T_e values go slightly below 0 °C ($-2.5\ ^\circ\text{C} \leqslant T_{e(min)} \leqslant -1.3\ ^\circ\text{C}$) during all considered days for cooling and solidifying about 7 kg of water. The methanol uptake (m_m) shown in Fig. 19 varies between about 4.2 kg on 14th June as a maximum and 0.27 kg on 19th June as a minimum out of the 5.99 kg (the maximum methanol that can be adsorbed into the system (M_m)). From 14th to 23rd of June, the average desorbed methanol amount ($m_m(d)$) is 3.275 kg out of the corresponding $M_m = 5.99$ kg (for NORIT RX3-Extra). Also $m_m(a)$ is about 3.223 kg (as average $m_m(a)$ for 10 days from 14th to 20th June). Therefore, the amount of produced ice is about 4.25 kg as the minimum on 19th June and 7 kg as the maximum on 15th June, respectively.

It is obvious from Fig. 19 and Table 12 that M_{ice} is between 4 and 5 kg such as on 18th, 19th and 20th June, that is because of the mass of water (m_w) in the evaporator is 7 kg. If m_w is reduced by 2 kg, i.e. to be 5 kg, the produced ice will be 5 kg on 18th, 19th and 20th June, as shown in Fig 20, at $T_{e(min)}$ equals −2.48, −1.95 and −1.58 °C with corresponding SCOP equals 0.126, 0.119 and 0.119, respectively.

The lowest COP, SCOP, ESCOP and SCP are 0.42. 0.119, 0.143 and 2.74 on the typical bad conditions day (19th June) as shown in Table 12.

In cold days (from 17th to 26th December), the system is also modeled to show the best performance can be obtained after the previous improvements. For this reason, the amount of water is increased up to 13 kg to show the maximum capability of the system for ice production. Figs. 21–23 and Table 13 represent the important operating and performance parameters.

Incident solar radiation (I_T) from 17th to 26th December on the tilted collector (collector tilt angle = 49.4°) is presented in Fig. 21. The highest and lowest $I_{T(max)}$ are about 1030 and 831 W m^{-2}, corresponding to total received solar energies of about 25.83 and 19.26 MJ m^{-2}

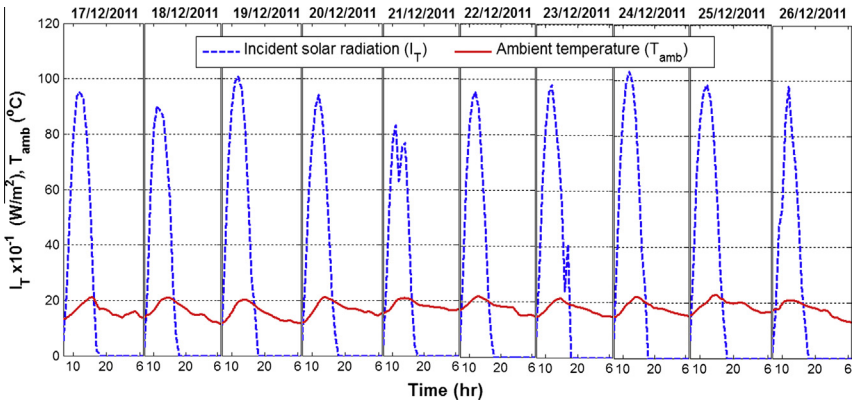

Fig. 21. Incident solar radiation on collector (I_T) and ambient temperature (T_{amb}) recorded during December 17–26, 2011.

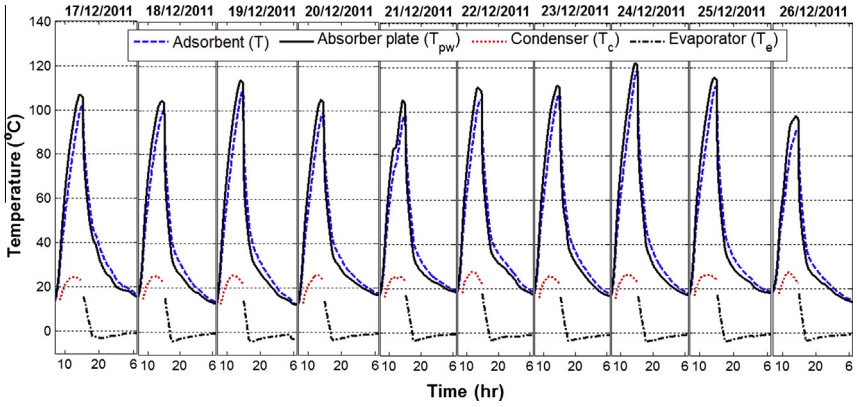

Fig. 22. Collector absorber (T_{pw}), adsorbent bed (T), condenser (T_c) and evaporator (T_e) temperatures calculated for the period 17–26 December 2011.

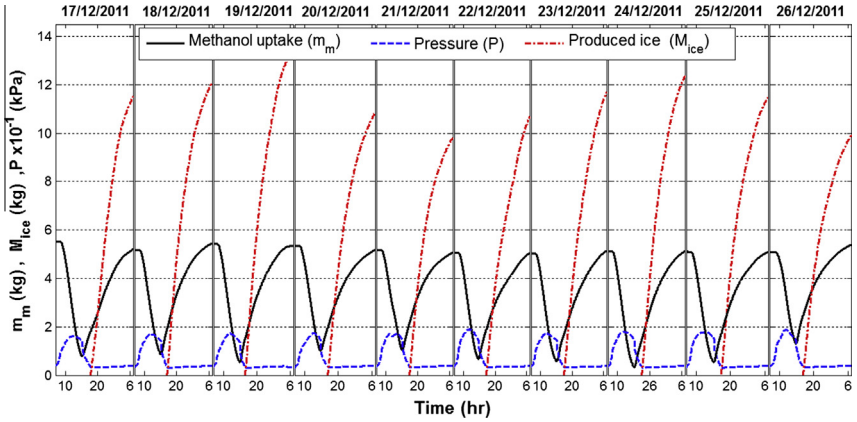

Fig. 23. Methanol uptake (m_m), adsorbent bed pressure (P) and amount of produced ice (M_{ice}) calculated for the period 17–26 December 2011.

Table 13
System performance for December 2011.

Date	17/12	18/12	19/12	20/12	21/12	22/12	23/12	24/12	25/12	26/12
COP	0.52	0.59	0.54	0.52	0.53	0.54	0.56	0.54	0.54	0.59
SCOP	**0.232**	**0.245**	**0.224**	**0.226**	**0.239**	**0.228**	**0.221**	**0.212**	**0.220**	**0.241**
ESCOP	0.251	0.265	0.254	0.258	0.264	0.258	0.255	0.241	0.246	0.279
SCP (W kg^{-1})	4.16	4.33	4.56	3.92	3.78	4.1	4.29	4.50	4.29	3.85
***M*$_{ice}$ (kg)**	**11.52**	**12.1**	**13.0**	**10.83**	**9.80**	**10.66**	**11.67**	**12.35**	**11.46**	**9.89**
$m_m(d)$ (kg)	4.73	4.32	4.90	4.33	4.13	4.37	4.46	4.79	4.57	3.79
$m_m(a)$ (kg)	4.39	4.58	4.81	4.41	4.01	4.35	4.55	4.76	4.55	4.08
P_e (kPa)	3.50	3.51	3.42	3.55	3.58	3.55	3.51	3.48	3.52	3.58
P_c (kPa)	14.45	15.14	14.72	14.79	15.64	16.91	15.41	16.01	16.41	16.38

Table 14
System predicted performance data for both June and December of 2011.

M_{ice} (kg)	COP	SCOP	ESCOP	SCP (W kg^{-1})	T_e (°C)
4.25–13	0.42–0.59	0.119–0.245	0.143–0.279	2.7–4.6	(−1.3)–(−4)

on 24th and 21st December, respectively. On 19th December, the total incident solar radiation is about 24.84 MJ m^{-2} instead of about 22.2 MJ m^{-2} at the same day if the collector tilt angle equals 23.6° (latitude of Dhahran); the increase is about 11.9% The maximum adsorbent temperature (T_d) is between 92.55 °C and 118.7 °C during these 10 cold days (from 17th to 26th December) as shown in Fig. 22. In the best weather condition day (19th December) $T_d = 108.72$ °C. $T_{e(min)}$ varies between −2.97 (on 17th December) °C and −4 °C (on 19th December); it does not go below −4 °C due to the large amount of water ($m_w = 13$ kg).

Fig. 23 and Table 13 show the important performance parameters during the cold days. m_m varies between about

5.5 kg as a maximum and about 0.34 as a minimum; the average desorbed and adsorbed amounts of methanol during those 10 days (from 17th to 26th December) are about 4.439 and 4.422 kg with the average desorption ($m_m(d)/M_m$) and adsorption ratios ($m_m(a)/M_m$) equal 74.1% and 73.82%, respectively. M_{ice} increases to an excellent value that reaches 13 kg on 19th December; the minimum M_{ice} is about 9.8 out of 13 kg on 21st December as shown in both Fig. 23 and Table 13 because of the higher minimum adsorbent temperature at the end of 21st December cycle ($T_a = 19.4$ °C) as shown in Fig. 22. Fig. 23 and Table 13 also show the system operative pressure is between 3.5 and about 17 kPa (absolute pressure) for December 2011.

These June and December results according to the pervious collector improvements may denote that the performance of the system during any day in a whole year is in between the values corresponding to $m_w = 7$ kg for June and $m_w = 13$ kg for December, as given in Table 14. M_{ice} is between 4.25 kg and 13 kg per m^2 of solar collector with the corresponding minimum evaporator temperature is between −1.3 and −4 °C, respectively. SCOP is also improved to be between 0.119 and 0.245 for Dhahran hot and cold days, respectively.

5. Conclusion

Performance of an intermittent solar thermal powered activated carbon/methanol adsorption cooling system is investigated in this research using the MATLAB modeling under weather data for Dhahran. The modeling study shows that:

- Thin stainless steel absorber tubes should be selected with suitable selective coating to improve both operative and performance parameters.
- Activated carbon NORIT RX3-Extra is more convenient for improving a solar adsorption ice-maker performance than the other known types; about 14.1 kg of NORIT RX3-Extra per m^2 of collector is the optimal mass for these improvements.
- In order to increase the desorption temperature and the amount of desorbed methanol for producing high amount of ice and improving the performance, the double glazing system should be chosen rather than TIM (Transparent Insulation Material) and single cover systems.
- Thermal insulation material used in the system is preferred to have quite low thermal conductivity. In addition, the increase of rear insulation of the collector enhances the performance. However the recommended thickness is 10 cm to avoid an exaggerated thickness of the collector.
- The collector tilt angle should be changed monthly to the suitable angle for collecting higher solar radiation. Furthermore, it is suitable to delay the start of heating time to be at 6 AM (solar time) in Dhahran summer days to give some extra minutes for enhancing cooling effect.

Finally, the results show that the system can produce from 5 kg of ice up to 13 kg by m^2 of collector under Dhahran climate conditions. Coefficient of performance (COP) and solar coefficient of performance (SCOP) are improved from about 0.42 and 0.12 as the minimum in the hot days to about 0.59 and 0.24 as the maximum in the cold days, respectively.

Acknowledgment

The support of King Fahd University of Petroleum and Minerals to carry out this investigation is acknowledged.

References

Critoph, R.E., 1988. Performance limitations of adsorption cycles for solar cooling. Solar Energy 41 (1), 21–31.
San, J.Y., Lin, W.M., 2008. Comparison among three adsorption pairs for using as the working substances in a multi-bed adsorption heat pump. Applied Thermal Engineering 28 (8–9), 988–997.
Wang, L.W., Wang, R.Z., Oliveria, R.G., 2009. A review on adsorption working pairs for refrigeration. Renewable and Sustainable Energy Reviews 13 (3), 518–534.
Askalany, A.A.M., Ismail, S.I.M., Ali, A.H.H., Morsyb, M.G., 2012. A review on adsorption cooling systems with adsorbent carbon. Renewable and Sustainable Energy Reviews, 493–500.
Alghoul, M.A., Sopian, K., Sulaiman, M.Y., Azmi, B., 2007. Review of materials for adsorption refrigeration technology. Anti-Corrosion Methods and Materials 54 (4), 225–229.
Srivastava, N.C., Eames, I.W., 1998. A review of adsorbents and adsorbates in solid–vapour adsorption heat pump systems. Applied Thermal Engineering 14, 707–7014.
Eric, J.H.U., 1998. A study of thermal decomposition of methanol in solar powered adsorption refrigeration systems. Solar Energy 52 (5), 325–329.
Vasta, S., Maggio, G., Santori, G., Freni, A., Polonara, F., Restuccia, G., 2008. An adsorptive solar ice-maker dynamic simulation for north Mediterranean climate. Energy Conversion and Management 49 (11), 3025–3035.
Zhao, H., Zhang, M., Liu, Z., Liu, Y., Ma, X., 2008. Mechanical and experimental study on freeze proof solar powered adsorption cooling tube using active carbon/methanol working pair. Energy Conversion and Management 49, 2434–2438.
Hassan, H.Z., Mohamad, A.A., Bennacer, R., 2011. Simulation of an adsorption solar cooling system. Energy 36, 530–537.
Leite, A.P.F., Grilo, M.B., Andrade, R.R.D., Belo, F.A., Meunier, F., 2007. Experimental thermodynamic cycles and performance analysis of a solar-powered adsorptive icemaker in hot humid climate. Energy Renewable 32, 697–712.
Medini, N., Marmottant, B., Golli, E.S., Grenier, P., 1991. Study of a solar icemaker machine. International Journal of Refrigerate 14, 363–367.
Ogueke, V., Anyanwu, E.E., 2009. The performance analysis of a solid adsorption solar refrigerator during collector cool-down and refrigerant evaporation/re-adsorption phase. Journal of Process Mechanical Engineering 223 (1), 11–19.
Li, M., Wang, R.Z., 2003. Heat and mass transfer in a flat plate solar solid adsorption refrigeration ice maker. Renewable Energy 28, 613–622.
Chekirou, W., Boukheit, W., Kerbache, T., 2007. Numerical modeling of combined heat and mass transfer in a tubular adsorber of a solid

adsorption solar refrigerator. Revue des Energies Renouvelables 10 (3), 367–379.

Critoph, R.E., Tamainot-Telto, Z., 1997. Solar adsorption refrigeration. Renewable Energy 12 (4), 409–417.

Li, M., Wang, R., Xu, Y., Wu, J., Dieng, A., 2002. Experimental study on dynamic performance analysis of a flat-plate solar solid-adsorption refrigeration for ice maker. Renewable Energy 27, 211–221.

Wang, R.Z., Li, M., Xu, Y.X., Wu, J.Y., 2000. An energy efficient hybrid system of solar powered water heater and adsorption ice maker. Solar Energy 68, 189–195.

Critoph, R.E., 1999. Adsorption refrigerators and heat pump. In: Burchell, T.D. (Ed), Carbon Materials for Advanced Technologies, Chap 10, ISBN 0-08-042683-2, pp. 303–340.

Duffie, J.A, Beckman, W., 2006. Solar Energy Thermal Processes. John Wiley& Sons. Inc..

Passos, E.F., Escobedo, J.F., Mrunier, F., 1989. Simulation of an intermittent adsorptive solar cooling system. Solar Energy 42 (2), 103–111.

Zhao, Y., HU, E., Blazewicz, A., 2012a. Dynamic modeling of an activated carbon–methanol adsorption refrigeration tube with considerations of interfacial convection and transient pressure process. Applied Energy 95, 276–284.

Anyanwu, E.E., Ezekwe, C.I., 2003. Design, construction and test run of a solid adsorption solar refrigerator using activated carbon/methanol, as adsorbent/adsorbate pair. Energy Conversion and Management 44 (18), 2879–2892.

Leite, A.P.F., Grilo, M., Andrade, R.R.D., Belo, F.A., 2004. Dimensioning, thermal analysis and experimental heat loss coefficients of an adsorptive solar icemaker. Renewable Energy 29, 1643–1663.

Zhao, Y., Hu, E., Blazewicz, A., 2012b. A comparison of three adsorption equations and sensitivity study of parameter uncertainty effects on adsorption refrigeration thermal performance estimation. Heat Mass Transfer 48, 217–226.

El-Sharkawy, I.I., Hassan, M., Saha, B.B., Koyama, S., Nasr, M.M., 2009. Study on adsorption of methanol onto carbon based adsorbents. International Journal of Refrigeration 32 (7), 06–011.

Henninger, S., Schicktanz, M., Hugenell, P., Sievers, H., Henning, H.M., 2012. Evaluation of methanol adsorption on activated carbons for thermally driven chillers part I: thermophysical characterization. International Journal of Refrigeration 35 (3), 543–553.